Agricultural and Forest Meteorology 256–257 (2018) 159–178

Contents lists available at ScienceDirect

Agricultural and Forest Meteorology

journal homepage: www.elsevier.com/locate/agrformet

Analysis of evapotranspiration components of a rainfed olive orchard during three contrasting years in a semi-arid climate

Chebbi W.[a,b,*], Boulet G.[b], Le Dantec V.[b], Lili Chabaane Z.[a], Fanise P.[b], Mougenot B.[b], Ayari H.[b]

[a] Université de Carthage/LR17AGR01 (GREEN-TEAM). INAT, Institut National Agronomique de Tunisie, 43, Avenue Charles Nicolle 1082, Tunis, Tunisia
[b] CESBIO, Université de Toulouse, (CNES/CNRS/IRD/UPS), 18, Av Edouard Belin, 31401 Toulouse, France

ARTICLE INFO

Keywords:
Eddy covariance
Sap flow
Evapotranspiration
Partitioning
Water stress
Rainfed olive

ABSTRACT

Evapotranspiration is one of the most important fluxes of the water budget in semi-arid areas. The estimation of actual crop transpiration is a major issue in those regions due to its remarkable impacts on the precision of irrigation scheduling, crop growth and yield. Rainfed olive trees are adapted to the southern part of the Mediterranean basin even though they are vulnerable to an increased number of drought spells that might occur under current climate change scenarios. This present paper studies both water and energy exchanges over a rainfed olive grove in semi-arid conditions. The hydrological functioning of sparse olive trees is difficult to characterize because of its low LAI. To better understand water exchanges within the Soil–Plant–Atmosphere continuum and better evaluate the evapotranspiration and its components, we combine data arising from eddy covariance, soil water content measurements and the sap flow method. First, we check the consistency of the evapotranspiration partitioning and water balance over three contrasted years: one wet and two dry. Total evapotranspiration (ET) from eddy covariance method compares well with the sum of the evaporation (E) generated from the surface soil moisture measurements and the transpiration derived from the sap flow method. The top meter soil water balance corresponds roughly to ET during the wet year but for the dry years there is an evidence of extraction by roots below the first meter of soil. Inter-annual variations of the transpiration and associated water stress levels are analyzed by the combined use of different types of eco-physiological (sap flow) as well as remotely sensed variables that can be monitored through proxi-detection (albedo, surface temperature, surface soil moisture). The amount and timing of vegetation stress are consistent throughout the various indicators. Consequently, this consistent set of data can be used to constrain a SVAT land-surface model capable of representing the various features of the water and energy budget for this specific land cover.

1. Introduction

Olive orchards are a key agro-system for the economy in the semi-arid regions of the Mediterranean basin, which are known for their irregular rainfall, high evaporative demand and frequent water shortages. In Tunisia, olive yards cover 1.8 million hectares with 65 million olive trees representing nearly 79% of the total tree-covered area and 34% of arable land ("Observatoire National de l'Agriculture," 2017,"Patrimoine et répartition - Office National de l'Huile de Tunisie," 2017).

Because of their physiological and morphological properties, olive trees can survive under semi-arid conditions. They are efficient for preventing soil erosion and desertification, in addition to their important role in improving the soil carbon balance. When external conditions are not favorable, like high temperature or drought, olive trees are able to balance water inflows and outflows by minimizing the loss of water from the surface to the atmosphere and maximizing root extraction (Fernández et al., 1997; Fernández and Moreno, 1999). Moreno et al. (1996) compare the water use efficiencies of irrigated and rainfed olive yards under the same climatic conditions. They show through heat pulse velocity sensors (inserted in one root of the tree) that rainfed olive trees transpire less than irrigated olive trees and can extract water through deep roots, whereas irrigated olive trees rely only on shallow roots. After a heavy rainfall, an olive tree that has not been irrigated for 3 months increases its transpiration by 40% without reaching transpiration rates of an irrigated tree in similar pedo-climatic conditions and decreases its transpiration quickly after a few days. This behavior proves that the olive tree carries out a conservation strategy in soil-water use. The roots in a rainfed orchard are mostly located at the surface near the trunk and grow deeper further away from the trunk (Fernández et al., 1991). The inter row spacing is adjusted to explore the maximum volume of soil in such systems (Fernández et al., 1991).

* Corresponding author at: Université de Carthage/LR17AGR01 (GREEN-TEAM). INAT, Institut National Agronomique de Tunisie, 43, Avenue Charles Nicolle 1082, Tunis, Tunisia.
E-mail address: chebbiwafa@outlook.fr (W. Chebbi).

https://doi.org/10.1016/j.agrformet.2018.02.020
Received 21 July 2017; Received in revised form 4 January 2018; Accepted 16 February 2018
Available online 20 March 2018
0168-1923/ © 2018 Elsevier B.V. All rights reserved.

Connor et al. (2014) explain how the row spacing affects the root density, water use and yield by combining model simulations of the response of olive trees yields to irradiation for different row spacing values. As a short term response to drought, the olive trees suffering from water stress can limit the relative water content of leaves, the photorespiration and the stomatal conductance (by closing the stomata) (Boussadia et al., 2008). During long drought periods, olive trees reduce their photosynthesis and thus their productivity (Ben Ahmed et al., 2007). When olive trees are exposed to severe drought, the roots reduce the efficiency of water transport through cavitation or suberification (Tataranni et al., 2015).

Despite the fact that olive trees are adapted to the past frequency of drought spells, they could be vulnerable to future climate changes if droughts are becoming more intense or more frequent. These severe weather conditions could threaten the resilience capabilities of the trees, alter soil moisture levels, biomass production and affect negatively fruit productivity in such water controlled systems. For instance, the region of Kairouan suffered from a substantial water deficit from 1998 to 2003 which led to a significant drop in the olive production by 95% in rainfed orchards. The average olive production of the previous 10 years was 837 tons while it was 75 tons in the year 2001 (Gargouri et al., 2008). To predict the quantities of olives produced in 2130, Viola et al. (2013) test the impact of future climate scenarios on the annual yield in olives by incorporating carbon assimilation during the development stage and by taking into consideration the effects of the vegetation water stress on the allocation of biomass. According to their study, the average yield of olive could decrease from 2.7 tons per hectare ($t\,ha^{-1}$) in 2010 to 1.9 $t\,ha^{-1}$ in 2130 as a result of reduction in rainfall (30%), in actual evapotranspiration (28%) and in carbon uptake throughout the growing season (27%). Similarly, Gómez-Rico et al. (2007) show that the fruit yield of a rainfed orchard is already four times smaller than that of an irrigated olive orchard. Hence, the relationship between the olive fruit size and ET (or water stress) is roughly linear (Bustan et al., 2015). A better comprehension of the underlying plant mechanism to resist to drought is therefore required so that we can study the influence of climate changes on these systems. Soil-Vegetation-Atmosphere Transfer (SVAT) models act as tools to simulate scenarios of energy and mass fluxes, in addition to their individual turbulent, radiative, conductive and water transfer components, and the stomatal control on transpiration (Boulet et al., 2000). Besides, when the projection of future climate is produced, they allow to explore past and future scenarios like more intense and longer drought periods and higher CO_2 concentration (Calvet et al., 2008), to study the year-to-year variability of water and energy balances in response to different climate conditions (Calvet et al., 1998) and to understand their partitioning: 1- into plant transpiration (T) and soil evaporation (E) and 2- into turbulent heat fluxes and available energy at the dry down scale. However, SVAT models require an important number of parameters and continuous meteorological data as inputs to replicate the plant functioning and its response to water stress. SVAT models also fail to reproduce the complex interaction of all the mechanisms governing soil evaporation. For example, when the top soil layer becomes dry during the second stage of evaporation, the water vapor transfers are not represented in SVAT models, especially when they occur in a very thin layer compared to the vertical discretization of the soil (Kuchment and Singh, 2009). Several physiological processes are also not accurately prescribed in most SVAT model schemes and are difficult to characterize. This is particularly true for the stomatal behavior (Arora, 2002), the energy storage in the trunk (Michiles et al., 2008), the cavitation of xylem conduits (Tognetti et al., 1996) and the root hydraulic lift (Caldwell et al., 1998). Neither of the experimental methods nor the modelling techniques discussed above are perfect; therefore a complete dataset is required to represent the inter-annual variability and the water and the energy balances components as well as to check the model ability to represent them.

To monitor the functioning of the olive tree, we need a good and suitable estimate of the transpiration (T). Hence, it is essential to determine the associated water budget components, such as deep drainage or the soil evaporation. E represents an important loss in sparse orchards (Boulet et al., 1997; Salvucci, 1997; Yamanaka and Yonetani, 1999) even through bare soils of semi-arid systems rarely evaporate at the potential rate except for a few days after precipitation.

Although the partitioning of ET between E and T is extremely important for understanding the hydrological cycle and for its modeling, (Reynolds et al., 2000), it is difficult to describe in these environments (Baldocchi et al., 2004) due to its high variability in space and time (Smith et al., 1995) and the difficulty to determine it accurately over such an heterogeneous area.

The estimation of transpiration of isolated trees can be achieved through three means: 1) by measuring T (Nicolas et al., 2005), 2) by measuring the ratio T/ET (Wang et al., 2010) or 3) by estimating E and ET through a residual analysis (Kelliher et al., 1992). Direct T estimates are obtained using the sap flow method (Granier, 1985), which is based on the sap flow heating dissipation by convection using sensors inserted into the tree trunk. The measured temperature difference between the heating source and the unheated sensor is directly proportional to the transpiration. The sap flow approach is praised for its efficiency to explore the relation between the root system and the canopy (sap circulation), its capacity to monitor transpiration continuously and on the long term for individual trees (Ben Aissa et al., 2009), its appropriateness for heterogeneous fields and its ability to describe physical and environmental controls on transpiration controls for individual branches or the whole tree. However, the sap flow requires the determination of the total sapwood area which often proves to be difficult and rather imprecise. The main limitation involves not only the scaling from the sensor to the tree, but also from the tree to the stand (Granier, 1987). Although transpiration chambers can determine directly the transpiration rate at the tree level, they are unable to represent the atmospheric conditions that prevail near the tree (Kölling et al., 2015). The chamber decreases the boundary layer and alters the water vapor in the confined volume. It is costly and also face a scaling-up problem (Kool et al., 2014). The ratio T/ET can be monitored through the isotopic method, but it is very expensive as well as difficult to implement (Williams et al., 2004). On the other hand, the flux-variance similarity partitioning proposed by Scanlon and Kustas (2010) consists in determining simultaneously the partitioning of water and carbon fluxes and requires only standard eddy covariance data. Hence, a continuous estimation of the vegetation water use efficiency (*WUE*) is required. The wide availability of eddy covariance data and the simplicity of the approach are the main benefits. Its efficiency is tested over isolated trees (i.e., Morgan Monroe State Forest) by Sulman et al. (2016) resulting in accurate values compared to the sub-canopy based method. The latter relies on comparing the eddy covariance data sampled from two different heights above the canopy to estimate the flux partitioning. Finally, we can deduce the transpiration rate from the estimates of the evapotranspiration and the soil evaporation. To do so, several methods of ET measurements and its components may be applied (Allen et al., 2011; Kool et al., 2014) such as lysimeter (Gebler et al., 2015), heat balance, isotope, chambers, eddy covariance (Baldocchi et al., 1988) and water balance method (Zeleke and Wade, 2012). E can be estimated by the soil weighting lysimeter (Scott et al., 2006), the soil heat pulse technique (Xiao et al., 2012) or the soil water budget method (Oren et al., 1998).

Nevertheless, the easiest solution to overcome the limitations of each method when applied separately is to combine two or more methods together. Thereupon, integrating the eddy covariance method with sap flow measurement aims to provide more robust estimates of E and T (Cammalleri et al., 2013). This method is applied over irrigated olive orchards (Er-Raki et al., 2009; Testi et al., 2004; Williams et al., 2004) showing promising results. For instance, Er-Raki et al. (2009) investigate irrigation practices by comparing localized drip and flooding irrigation techniques. They show that the combined use of sap

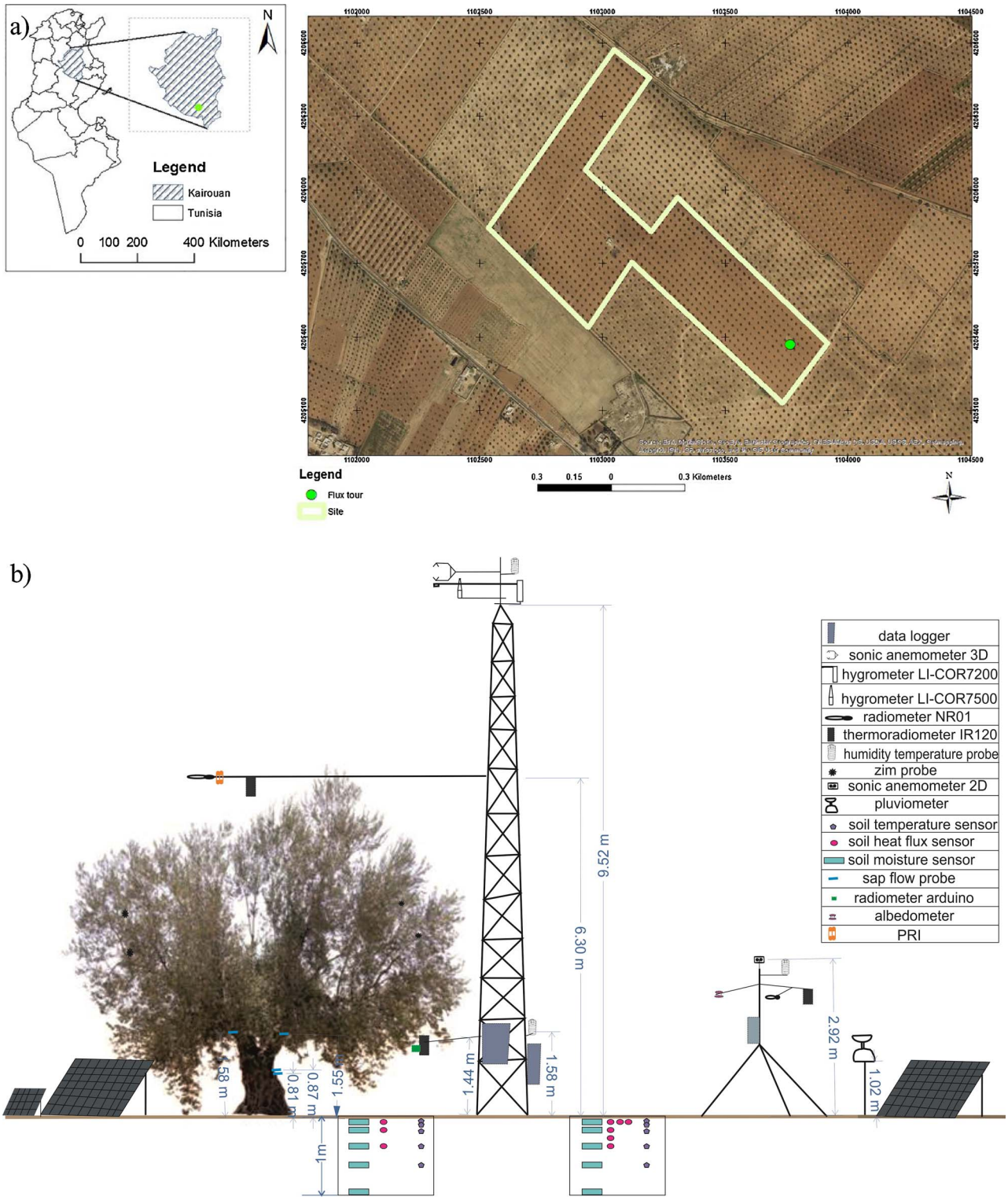

Fig. 1. Schematic of the study area and the site instrumentation.

flow and eddy covariance methods is a way to provide more robust estimates of E and T. However, the ratio T/ET is sometimes higher to 1 due to the transpiration scaling approach. Testi et al. (2004) show that even though the eddy covariance method is consistent with the water balance measurement for the three-years study, there is a lack of energy balance closure at low wind speeds, and thus at low turbulence, and also at strong wind speeds due to the low measurement frequency. Williams et al. (2004) focus on the good results of partitioning using these methods especially for daily maximum ecosystem gas exchange. The isotope is a worthy approach for partitioning over heterogeneous land that does not require scaling. The main limits of the eddy covariance are: 1) the different scales of measurements, 2) the lack of energy balance closure because of the location of the soil heat flux measurements (exposed or shaded) and the energy storage within the biomass. Therefore, in the present work, the choice of using the eddy covariance method is explained by the large extent of the experimental rainfed

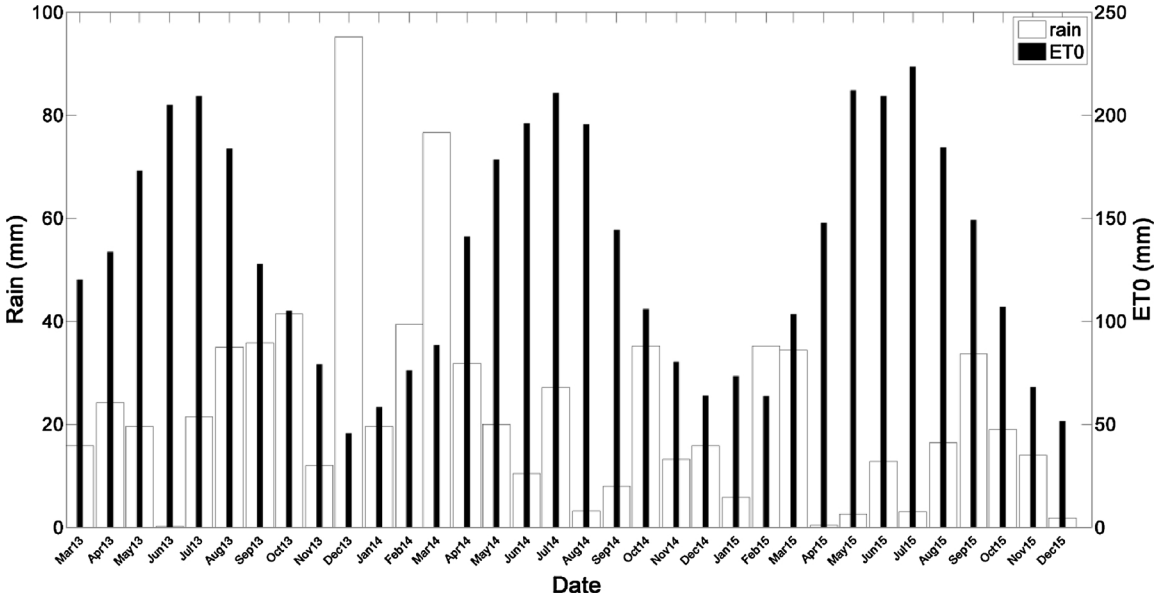

Fig. 2. The rainfall and the reference evapotranspiration in the study site.

olive orchards. To better understand the partitioning of water fluxes, we choose to combine the eddy covariance and the sap flow. This chosen rainfed olive orchard is characterized by its low fraction cover (7%). The semi-arid conditions in this study result in a fast drying of the top soil layer and a fast decrease of the evaporation rate. Under such conditions, the plant is subject to high water stress levels which increase the competition between the two evapotranspiration components for the water use.

Apart from transpiration itself, it is important to monitor the plant response to drought; therefore, assessing the plant water stress is a key step in this process. To do so, indicators obtained from in-situ or satellite remote sensing can be used. Those indicators are often based on the near-infrared and the visible spectral bands. Jackson et al. (1981) and Zarco-Tejada et al. (2012) suggest that the canopy temperature measured with a thermal radiometer in situ, or (T_v-T_a), the difference between the temperatures of the vegetation and the air temperature, is a good baseline to monitor water stress. In fact, the stomatal closure leads to an increase in leaf temperature because of the reduction of transpiration especially for high water stress levels. Kool et al. (2016) demonstrate that the limits of the approach can be due to the variation of (T_s-T_a) with the soil or the plant water content, the shade or the position of the sensor (in the inter-row or below plantation). Some other authors have shown the high frequency fluctuations of the surface temperature measurements (Lagouarde et al., 2000). This indicator does not take into account the short term fluctuations of the climatic forcing. To overcome this problem, it is advisable to use the surface to the potential surface temperature difference derived from a model as described by Boulet et al. (2007) or to divide the difference (T_s-T_a) by the global radiation (Rg) as proposed by Amano and Salvucci (1999). Since high frequency fluctuations, as a result of turbulent conditions, are likely to be distributed evenly around the mean, monitoring trends of this variable is promising. The surface temperature can be easily achieved by remote sensing and can be spatialized over large scales.

Nowadays, there exists no complete set up to study the energy budget components and to track the stress over a sparse rainfed olive orchard in semi-arid lands. Therefore, in this study, we build a complete experimental protocol and evaluate the performance as well as the consistency of the resulting data base through the following methodological framework over three contrasting years: 1) securing E/T partitioning through total and component flux evaluation, 2) relating plant water use to soil moisture change in the top soil to investigate the link between root uptake and transpiration at seasonal level, and 3) verifying the consistency between the various indicators that monitor the components of water stress levels. First, we present a three-year comparison between the evapotranspiration measured using the eddy covariance method and the sum of the evaporation generated from the model and the transpiration derived from sap flow measurements. Then, we study the surface energy and water budget components. Finally, in order to track early plant water stress, we test the consistency of the in-situ and the remote sensing indicators.

2. Materials and methods

2.1. Site description

Our study is conducted in olive orchards covering an area of 39 ha in the plain of Kairouan, central Tunisia (35°18′17.14″; 9°54′56.62″) (Fig. 1). It is a semi-arid region with average annual precipitation of 300 mm. Rainfall varies largely in space and time with a severe drought of 108 mm in 1950 and a flood-generating peak of 700 mm in 1969 (hydrological years: September to August). It has a marked seasonal pattern (a wet season from October to April and a dry season from May until September). The daily average temperature is about 19 °C with a minimum of 10 °C in January and a maximum of 28 °C in August. The mean annual reference evapotranspiration is about 1600 mm. The monthly evapotranspiration and the rainfall in the study area are shown in the Fig. 2. Olive trees in this site were planted with a spacing of 20 m resulting in a fractional vegetation cover of about 0.07. This tree density is comparable to the olive tree density of rainfed olive orchards in central region of Tunisia (Jackson et al., 2015), i.e. from 8 m in the north to 25 m in the south. Trees are 80 years old. The soil is loamy sand (88% sand, 8% clay, 4% silt; density: 1.65 g cm^{-3}).

The instrumentation documentation described by Chebbi (2017) provides more details about the instruments installed to obtain both high and low frequency measurements, and the Fig. 1 shows the experimental set up which is composed of:

- An eddy covariance mast installed near one of the four trees instrumented with sap flow sensors, at the center of the orchard. The eddy covariance sensors are mounted at the top of the tower which is about 10 m above the ground. The average canopy height is about 5 m.
- A bare soil mast at the inter-row with wind measurement at a height of 2.52 m.

- A pluviometer (Campbell S. SBS-500, USA).

2.2. Micrometeorological fluxes measurements and energy-balance closure

2.2.1. Net radiation and soil heat flux

Net radiation over the olive tree (*Rnv*) is measured with a NR01 net radiometer (Husekflux, Delft, the Netherlands) placed at 6.5 m above the ground and about 0.4 m above the olive tree canopy. The NR01 is a hemispherical four-component net radiometer consisting of two SR01 pyranometers and two IR01 pyrgeometers. Similarly, net radiation (*Rns*) is determined over the bare soil with an NR-Lite Net Radiometer (Kipp and Zonen, Delft, Holland). The total net radiation is estimated by weighting the bare soil and the canopy measurements with the fraction cover.

$$Rn = Rnv*f_c + Rns*(1\text{-}f_c) \quad (1)$$

Where *fc* is the total fraction of vegetation cover (0.07 - see section 2.2.2).

Here, *Rnv* represents the combined net radiation from the vegetation and the soil beneath the tree crown. The net radiation measured by the NR01 sensor is determined by the fraction of the radiometer view that is occupied by soil versus vegetation, expressed as

$$Rn_{\ radiometer} = Rnv*f_v + Rns*(1\text{-}f_v) \quad (2)$$

The factor f_v is the fraction of canopy cover in the radiometer view. Its value (0.85) is calculated using hemispherical photography image processing. The latter was acquired at the same place as the radiometer in order to represent exactly what the radiometer observes.

Albedo is also measured above bare soil using an albedometer (Skye Instruments Ltd, Llandrindad Wells, Powys).

Heat flux plates (Hukseflux HFP01, Delft, the Netherlands) are placed at a depth of 2 cm: 2 plates below the tree and 4 plates below bare soil. For the bare soil and the soil under the tree, 3 plates are also inserted at depths roughly equal to 5, 15 and 30 cm.

The surface soil heat flux is calculated by correcting the soil heat flux at the 2 cm depth for the 0–2 cm heat storage. By doing so for the 4 heat plates at the bare soil site and the 2 plates below the canopy, one computes the soil heat flux in unshaded (*Gs*) and (*Gv*) conditions, respectively.

Soil temperature, measured by temperature probes (Campbell S. TH108, USA), is recorded at 2, 5, 15, 30 and 50 cm depths at two locations: below bare soil and below the tree.

The total soil heat flux is estimated by the following equation:

$$G = Gv*fc + Gs*(1\text{-}fc) \quad (3)$$

2.2.2. The eddy covariance system

CO_2, latent and sensible heat flux measurements are recorded on the tower about 5 m above the top of the olive canopy (Baldocchi et al., 1988). A 3D sonic anemometer (Campbell S. CSAT3, USA) measures the fluctuations in the wind velocity components and air temperature. To estimate concentrations of water vapor and carbon dioxide, we install a closed-path infrared gas analyzer (Campbell LI7200, USA) from May 3, 2012 to August 26, 2013 and an open-path infrared gas analyzer (Campbell LI7500, USA) from August 26, 2013 to December 31, 2015. The 20 Hz sampled measurements of wind speed and concentration are made on CR3000 data loggers which enable to store large raw data files. Air temperature, surface temperature vapor pressure deficit, CO_2 flux, rainfall and wind speed are recorded every 30 min from the experimental site.

Data quality control from the EC system is analyzed using the "eddypro" software (open source software application developed, maintained and supported by LI-COR Biosciences). We use the software's default settings for time-series checks, low and high pass filtering, density fluctuations, sonic anemometer tilt correction with double rotation.

The REddyProc tool ("Biogeochemical Integration | Services/REddyProcWebGapFilling," 2011) is used to fill gaps of meteorological and processed eddy covariance data. This method consists in filling water fluxes gaps required to estimate monthly balances using data with similar meteorological conditions defined via the global radiation (*Rg*), the air temperature (T_a) and the vapor pressure deficit (*VPD*).

Post-processing includes forcing of the energy balance closure. The energy balance equation can be approximated by:

$$Rn\text{-}G\text{-}LE\text{-}H = 0 \quad (4)$$

According to many studies, the energy balance with the EC system is usually characterized by the lack of closure for many reasons (instrument malfunction, low and high-pass filtering errors…). The closure of the energy balance for the whole three-year study is first assessed using half hourly values of the energy balance components for each day (see the Fig. 1 in the supplemental section). The slope is about 0.91, the intercept is about 12.06 W m^{-2} and the coefficient of determination is 0.75. As shown by Anderson and Wang (2014) and Leuning et al. (2012), the energy balance closure is improved when aggregated to daily totals. The slope is then about 0.98 the intercept is 16.6 W m^{-2} and the coefficient of determination is 0.83. Since the slope is very close to 1 and the offset close to zero, we assume that little correction is required and that the raw measured heat fluxes are relevant. However, to provide a first guess of the measurement uncertainty, we propose an investigation of other estimates leading to energy balance closure: one obtained from the Bowen ratio correction method, and the other one from the residual method (Teixeira and Bastiaanssen, 2012). The latent heat flux according to the residual method LE_{res} assumes that only *H* is correctly measured:

$$LE_{res} = Rn\text{-}G\text{-}H_{EC} \quad (5)$$

The Bowen ratio method assumes that turbulent energy filtering affects both *H* and *LE* similarly and that the Bowen ratio β is correct.

The latent heat flux and the sensible heat fluxes obtained with the Bowen ration correction are as follows (Teixeira and Bastiaanssen, 2012):

$$LE_{BR} = \frac{Rn - G}{1 + \beta} \quad (6)$$

$$H_{BR} = \frac{Rn - G}{1 + \frac{1}{\beta}} \quad (7)$$

Where γ is the psychometric constant (kPa °C^{-1}), ΔT is the vertical temperature gradient (°C) and Δe is the vertical water vapor pressure gradient (kPa).

As proposed by Sanchez et al. (2008), three estimates will be derived: one with no closure correction, and two by applying both closure corrections.

We also estimate the footprint, i.e. the relative contribution of each element of upwind surface area to the measured vertical fluxes, using the method of Horst and Weil (1994). Our study aims to determine the vegetation fraction cover in the flux source area of each 30 min and thus the area contributing to the measurements that originates from the trees. This precise fraction cover is then used to calculate the whole available energy *Rn-G* since we estimate separately *Rn-G* for the vegetation and *Rn-G* for the bare soil. We plot all the tree crowns of the area, georeference them using a high resolution image of the orchard acquired by the Pléiades satellite on April 27, 2012, and apply a layer mask (0 for bare soil and 1 for olive tree). The relative fraction cover of the trees within the footprint varies from 0.003 to 0.011. Since it is close to the average fraction cover (0.07), the latter value is selected for the rest of the study.

2.3. Sap flow, root density and soil water content measurements

2.3.1. Sap flow

Sap flow measurements are performed using the heat dissipation technique, HDT (Granier, 1985). The mean sap flow density according to Granier (1985) is expressed as follow:

$$u\ (m\ s^{-1}) = 119*10^{-6}K^{1.231} \quad (8)$$

In which $K = \frac{\Delta T_{max} - \Delta T}{\Delta T}$ is a dimensionless flow index depending on $\Delta Tmax$ (when the sap flow velocity is minimal) and ΔT (the measured temperature difference). We choose a cyclical heating system switches, from ("on") to ("off") and then ("off") to ("on"), every 24 h in order to determine $\Delta Tmax$ accurately. This adjustment is necessary in these semi-arid environments with high diurnal thermal amplitude as discussed by Do and Rocheteau (2002). An analysis of the day "off" flux demonstrates the impact of the ambient temperature on the sap flow measurement (data not shown).

2.3.1.1. Scaling from sensor to tree. The total sap flow is computed as:

$$F_d\ (L\ s^{-1}) = u*SWA \quad (9)$$

In which *SWA* (SapWood Area) is the whole cross-sectional area of the sapwood. (9) scales the punctual probe measurements to the whole conductive stem section. To estimate the *SWA* and to study the impact of varying this parameter (sensitivity analysis) on the retrieved transpiration, two methods were performed. According to Charfi Masmoudi et al. (2011), the *SWA* of a young olive orchard depends on the total stem section St (cm^2):

$$SWA = 0.789\ St - 0.135 \quad (10)$$

Ramos and Santos (2009) establish a linear relationship between the *SWA* of 80-year-old rainfed olive orchard and the trunk diameter T_d (m):

$$SWA = 0.1702T_d - 0.0076 \quad (11)$$

Since, in literature, the *SWA* varies with the age of the plantation, the sap flow is calculated using Eq. (11) which corresponds to trees of the same age-group.

To estimate sap flow rate at the site scale, 4 trees are equipped with TDP50 sensors. The position of the trees is chosen according to the footprint analysis. Two sensors are inserted on each side of the tree trunk, on both north and south facing slopes, in order to take into account the heterogeneity of the sap flow in the trunk due to sun orientation. Both probes are insulated to minimize the direct sun exposure. In the instrumented tree near the flux tower, two additional sensors are installed on two main branches to verify the balance of sap inflows and outflows at the trunk level. The measurements cover the period from March 3, 2013 to December 31, 2015.

2.3.1.2. Scaling from tree to orchard. The whole-tree sap flow (l day^{-1} $tree^{-1}$) calculation is determined as the mean of the two sensors of each tree using Eq. (9). Finally, to estimate the transpiration in mm per day of the whole orchard, different upscaling methods are carried out. Trunk section is measured for a sample of 25 trees around the tower. One estimate is obtained by attributing the sap flow values of each instrumented tree to all trees having similar allometry. A second estimate is obtained by calculating the average value of the 4 sap-flow trees to the whole sample. The average of both estimates is supposed to be representative of the orchard transpiration. The daily transpiration of the orchard (mm day^{-1}) is the transpiration (T) multiplied by the number of trees per square meter of soil. 50% of the sap flow data is not measured due to methodological constraints, which can be problematic for the partitioning of the energy balance at monthly and yearly scales. Therefore, a gap-filling method based on the reference evapotranspiration is applied. The missing data on day j are gapfilled from the data acquired on days j-1 and j + 1:

$$T_j = \left(\frac{(T/ET0)_{j-1} + (T/ET0)_{j+1}}{2} \right) * ET0_j \quad (12)$$

Where ET0 is the reference evapotranspiration (Fao-56 reference crop) (Allen et al., 1998).

Eventually, as an attempt to monitor the plant water stress, T is scaled up to a maximum theoretical value and the potential transpiration (T_p) is computed with the Penman Monteith equation as described by Bailey et al. (1993). Therefore, an index of plant water status is the Potential Transpiration Index (*ITP*):

$$ITP = 1\text{-}(T/T_p) \quad (13)$$

2.3.2. Root density measurements

Root density is also determined around the instrumented tree using the auger method proposed by Schuurman and Goedewaagen (1971). First, samples are taken in two directions (North, South) at the surface and at depths 20, 40 and 60 cm, at 1, 3, 5, 7 and 9 m away from the trunk, respectively. The samples are then sieved with a very small mesh square. Finally, the root surface is calculated with a dedicated imaging software (Mesurim) after scanning. Fig. 4 shows that the highest root density values are recorded between 0 and 40 cm in the first 3 m away from the trunk and between 40 and 60 cm at 9 m from the trunk. This increase in the root density can be explained by an overlap area with the roots of the opposite olive tree.

2.3.3. In-situ remote sensing measurements

Several other remote-sensing indices are also recorded continuously: the surface temperature of the vegetation (T_v) and the soil (T_s) are recorded over the period of study using a thermal radiometer IR120 (Apogee Instruments Inc., Logan, UT, USA) at nadir, one being located above the instrumented tree, and the other above the bare soil. The vegetation stress index (IS_v), which is the difference between T_v and T_a divided by *Rg*, is used to derive a water stress index of the plant and the soil controlled evaporative index (IS_s), which is the difference between T_s and T_a divided by *Rg*, is used to distinguish the two evaporation stages (Amano and Salvucci, 1999). A very small part of the bare soil and the trunk are also seen by the sensor above the tree. Since this fraction is very small, we assume that the evolution of the TIR index IS_v is mostly sensitive to the vegetation water stress. The photochemical reflectance index (PRI) was also recorded from June 20, 2014 to December 31, 2015 above the crown of the instrumented tree (not shown).

2.3.4. Soil water content measurements

The soil water content (*SWC*) is continuously monitored with ML2X (Delta-T Devices Ltd, Cambridge, UK) soil moisture probes for two profiles, one close to the bare soil mast, and the other below the tree overlooked by the tower. For each profile, five probes are installed at depths 5, 15, 30, 50 and 100 cm (Fig. 3). To calibrate the probes, gravimetric soil moisture samples are taken at the same depths and at various dates of the sampling period.

The plant available soil water (*PAW*) could thus be obtained from *SWC* as:

$$PAW = (SWC\text{-}\theta_{wp})/(\theta_{fc}\text{-}\theta_{wp}) \quad (14)$$

Wilting point (θ_{wp}) (5.0%) and field capacity (θ_{fc}) (14.9%) in the top layers (0–40 cm) are determined using pedotransfer functions from Wagner et al. (2001).

The choice of *PAW* between 0 and 40 cm is based on the root density distribution shown in Section 2.3.2. *PAW* is used to define a threshold of severe soil water scarcity. When the *PAW* lies between 40 and 60%, the plant is considered under moderate water stress conditions. However, it is under high water stress conditions if the *PAW* is lower than 40%, as described by Phillips et al. (1984).

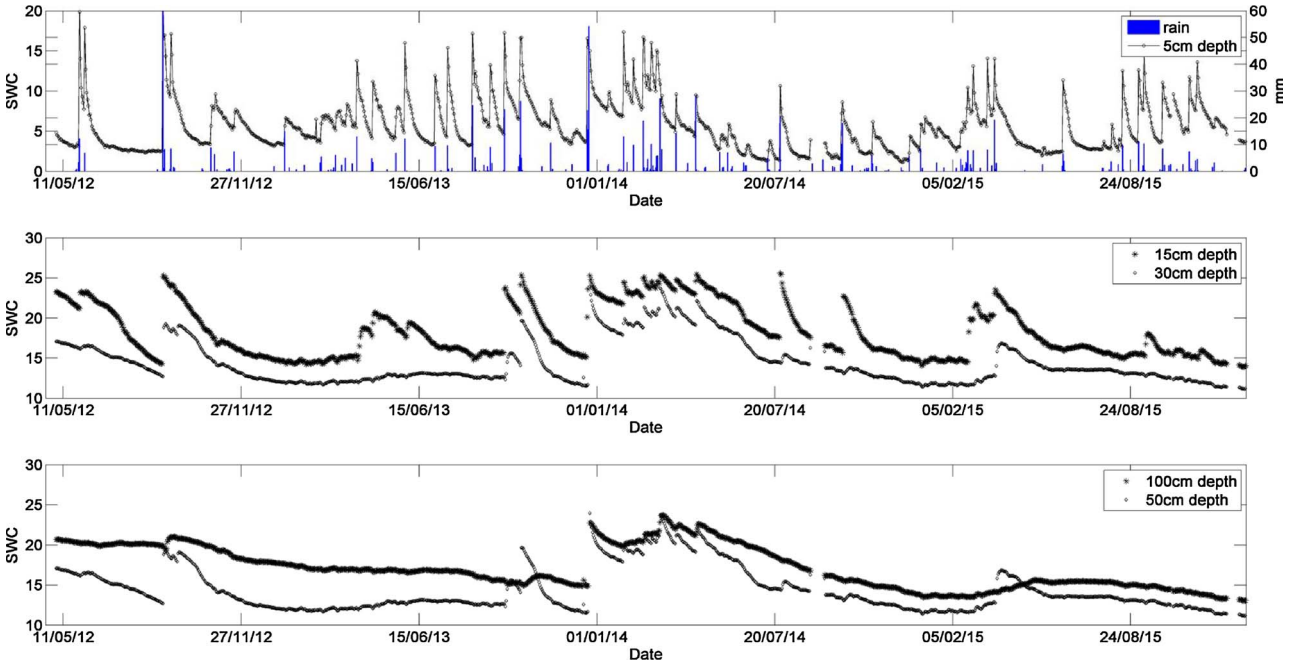

Fig. 3. The soil water content in the study site at different depths.

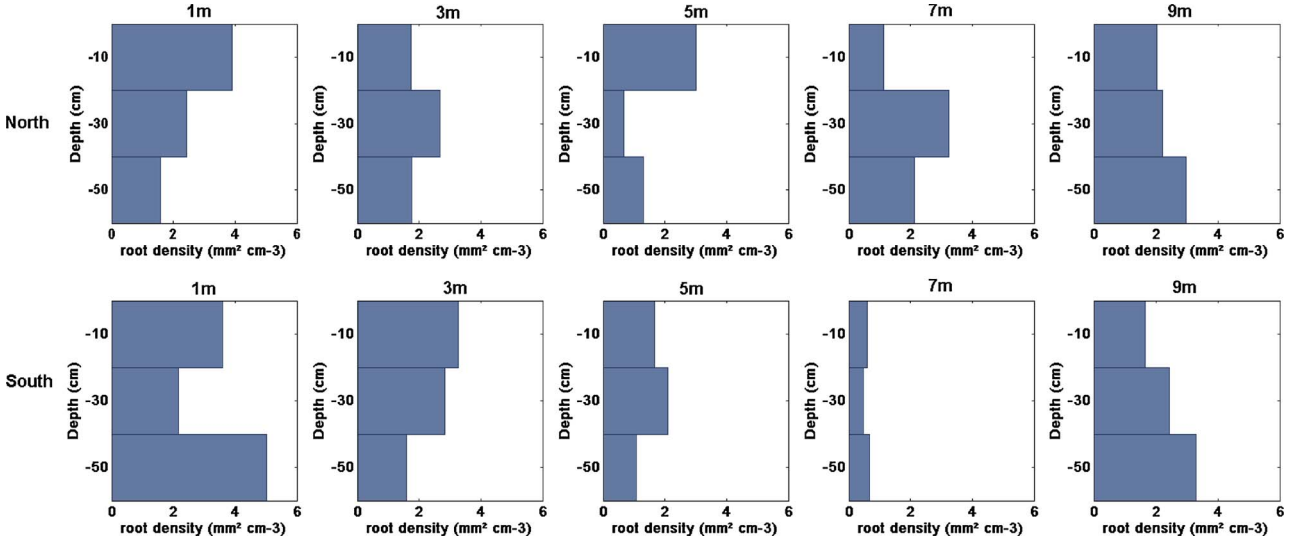

Fig. 4. The root density profiles following two directions and at different distances from the trunk.

2.4. Evaporation estimation

In this study, we used surface volumetric soil water content measured by the ML2X probes near the tree and in the bare soil to estimate soil evaporation E. The approach relies on an evaporative efficiency βe, the ratio between the actual and the maximum evaporation rates:

$$E = \beta e * E_{max} \quad (15)$$

Where E_{max} is the maximum evaporation.

Several formulations relate βe to the surface soil moisture. We test three of them. One of them is the analytic formulation of Merlin et al. (2011).

$$\beta e = \begin{cases} \left[\frac{1}{2} - \frac{1}{2}\cos(\pi\theta_d/\theta_{max})\right]^p & for\ \theta_d \le \theta_{max} \\ \beta e = 1 & for\ \theta_d > \theta_{max} \end{cases} \quad (16)$$

Where θ_d is the water content d (i.e. the topsoil providing most evaporation water), θmax is the soil moisture at saturation, and p is a shape parameter depending on the soil texture.

Another evaporative efficiency described by Song et al. (2016) is tested. It also depends on the surface soil moisture at the top soil layer.

$$\beta e = \frac{2}{1 + (\frac{\theta_d}{\theta_{fc}})^{-2}} \quad (17)$$

The FAO 56 model for bare soil evaporation (Allen et al., 1998) is also evaluated. The two stages of evaporation are distinguished using a coefficient (K_r) that depends on the soil water content as:

$$\beta e = \frac{TEW - 0.1 * \theta_{fc} - \theta_d}{TEW - REW} \quad (18)$$

Where TEW and REW are the total and the readily evaporable water, respectively, in mm.

The rough estimate of the uncertainty in E is achieved by using various combinations of $Emax$ and βe values: we test the potential evapotranspiration, as described by Boulet et al. (2000) and the

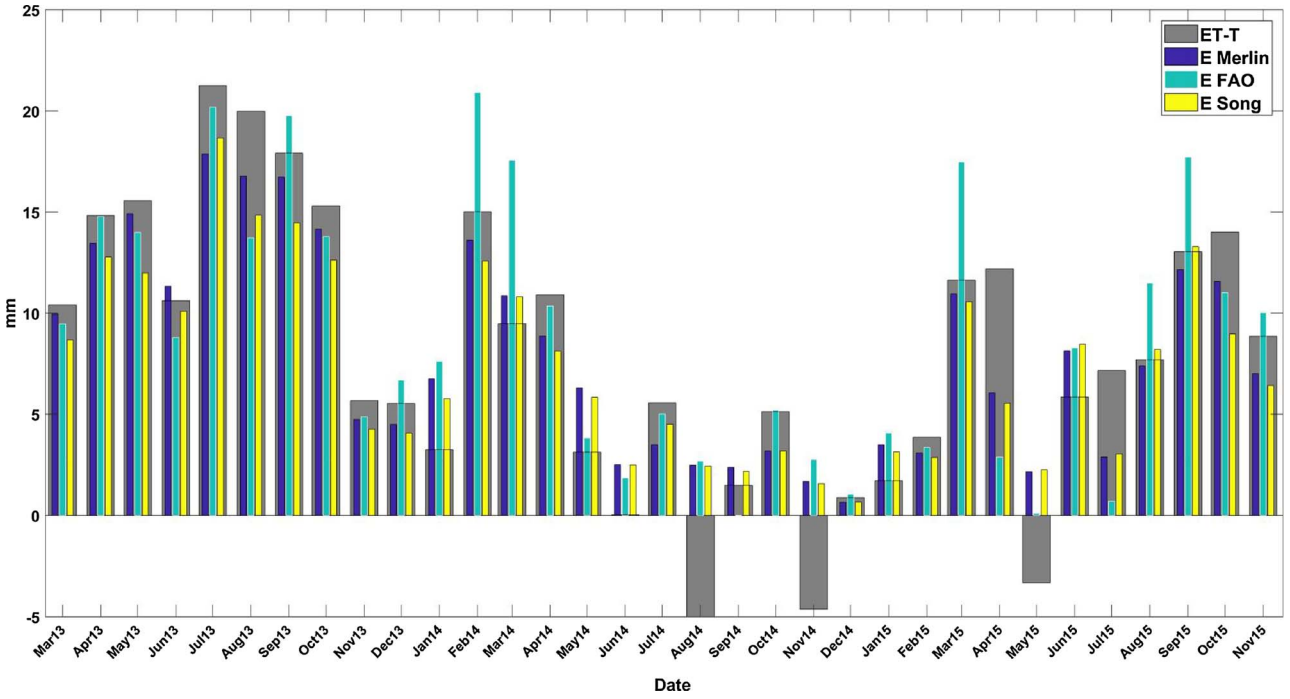

Fig. 5. Comparaison between the monthly evaporation by three models (Merlin, FAO and Song) and the difference between the evapotranspiration from EC and the transpiration from the Sap flow (ET-T).

reference evapotranspiration (Fao-56 reference crop), as described by Allen et al. (1998). For each of these methods, the soil evaporation efficiency is calculated with three values of p (1; 1.5; 2) for Eq. (16) or various values of the wilting point (i.e., from 0.1 to 0.3) for Eq. (18) and at two different depths (5 cm; 15 cm). To select parameters which produce the best fit, we compare the soil water content measured in situ with a simulated soil water content based on surface water budget while varying the main parameters of the evaporation models (p, θ_{wp}). The simulated soil water content is calculated through a surface water balance using Eq. (19) in order to optimize the evaporation model.

$$\theta_{day+1} = \theta_{day} + \frac{E_{day}}{d} \tag{19}$$

The βe parameters and d are determined using an optimization which is based on the minimization of the Root Mean Square Error (RMSE) between the modeled and the observed soil moisture using Eq. (19). We select parameters which produce best fit.

3. Results

3.1. Water balance

Our study is conducted over three contrasting hydrological years (from September to August). Total precipitation is about 116 mm in 2013 (dry year), 413 mm in 2014 (wet year) and 180 mm in 2015 (dry year). Since we measure soil water content until 1 m depth, we try to evaluate the water balance closure for this depth as an attempt to check the year-to-year variability, the consistency between the EC data, and the amount of water extracted from the top meter of soil where most roots are located.

If one neglects the drainage considering the results of one year measurements of the deep drainage using lysimeter (Decagon Devices Inc., Pullman, WA) at 1 m depth (not shown) and the increase of the percentage of clay with depth which increases the field capacity towards 1 m depth, the seasonal water balance can be approximated as the sum of the soil water storage at 1 m (ΔS) and the evapotranspiration (ET) from EC measurements versus the rainfall. The seasonal cumulative sum of rainfall is mostly lower than the cumulative sum of ΔS + ET, especially during the dry periods. The increase of the deficit is significant under surface water limiting conditions. In the summer of 2014, ΔS + ET exceeds the amount of rainfall by 134 mm. In the autumn of 2014, the precipitation with a total seasonal amount of 56 mm. This is the lowest value recorded in autumn during the study period. It does not meet the sum of the extractable water at the top meter of soil and the water lost to the atmosphere by evapotranspiration (i.e, 143.8). Similarly, this deficit is about 67 mm, 25 mm, 68 mm and 77 mm during the autumn of 2014, the spring the summer and the automn of 2015, respectively. Throughout the dry year 2013 (i.e., the winter, the spring and the summer), ΔS + ET always exceeds P, but during wet periods (i.e, the autumn of 2013, winter-spring of 2014 as well as the winter of 2015), the cumulative sum of rainfall is approximately equal to the cumulative sum of ΔS + ET. When an amount of 70 mm precipitation fall, the top meter soil balance closure is achieved.

3.2. Evapotranspiration partitioning

After checking the consistency at seasonal scale, we focus on the analysis of the daily (Fig. 7) and monthly (Fig. 6) evapotranspiration and its components. To do so, the monthly and daily totals of the evaporation from the evaporation models and the transpiration from the sap flow are compared to the corresponding evapotranspiration eddy covariance. Fig. 5 shows the evaporation derived from the three methods: Merlin, Song and the FAO. The Song method gives evaporation rates similar to the Merlin evaporation modeled. The monthly evaporation rates derived from the three models based on the observed surface soil moisture time series after calibration are comparable to the monthly difference between the evapotranspiration from eddy covariance and the transpiration from the sap flow measurements. The correlation coefficients are 0.85, 0.83 and 0.84 for the Merlin, the FAO 56 and the Song models, respectively. The RMSE is 0.012, 0.013 and 0.014 for the Merlin, the FAO 56 and the Song models, respectively (see Fig. 3 in the supplemental section). However, the monthly evaporation derived from the FAO linear model tends to be higher. In what follows, the evaporation derived from the Merlin model will be kept. The Merlin model, where β_e is calculated with $p = 1$ and $d = 5$ cm, produces the

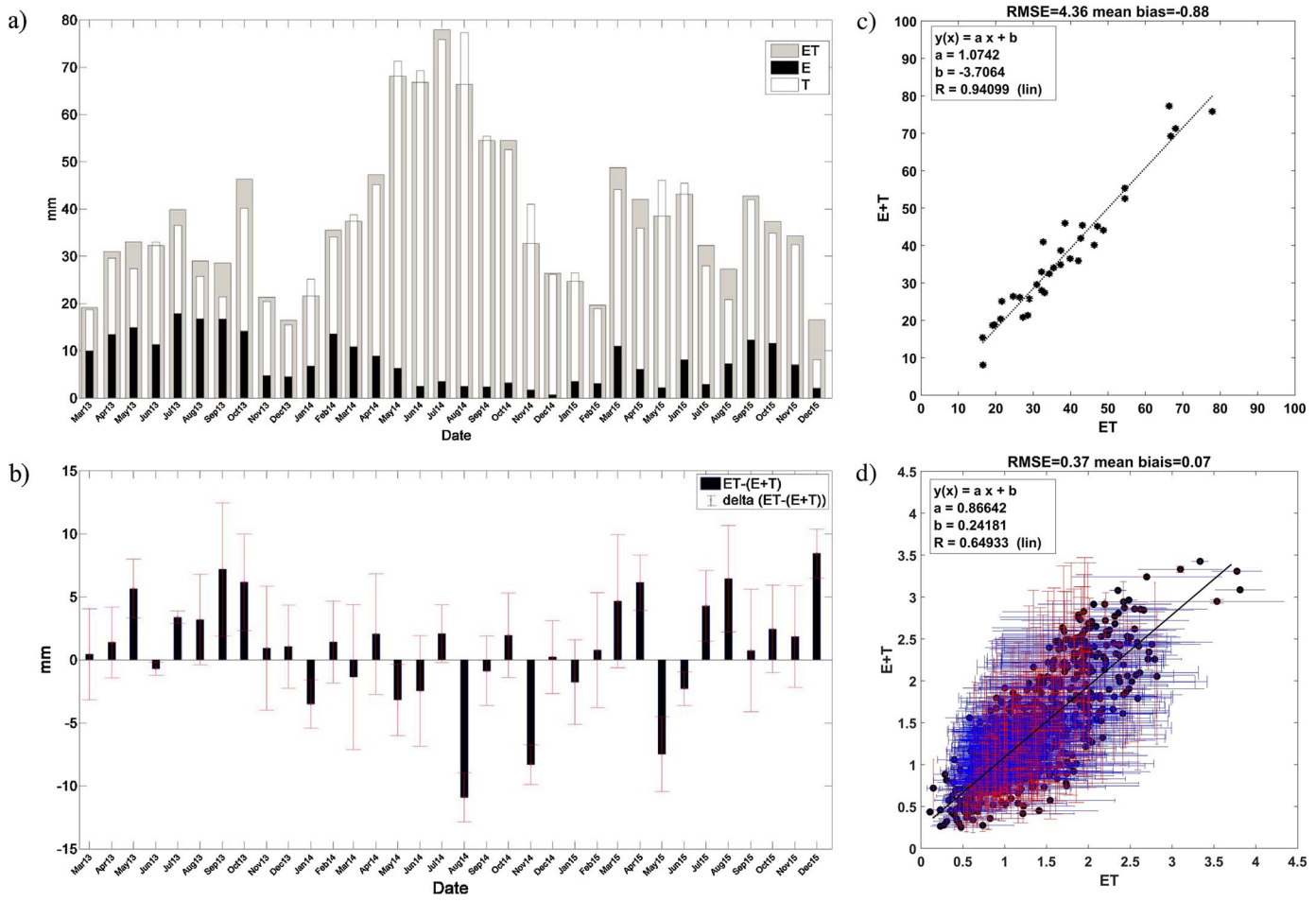

Fig. 6. a) Monthly evapotranspiration (ET) partitioning into transpiration (T) and evaporation (E); b) the difference between ET and E + T and its corresponding uncertainty; the relationship between ET from eddy covariance and the sum of the transpiration from the sap flow and the evaporation from the model at the monthly scale (c) and at the daily scale with vertical error bars that corresponds to the uncertainty of E + T and horizontal error bars that corresponds to the uncertainty of ET (d); a is the slope and b is the intercept, R is the coefficient of determination and RMSE is the Root Mean Square Error.

best fit with the modeled soil water content using Eq. (19) with a coefficient of determination equal to 0.85. Fig. 5 supports this choice.

A comparison of monthly ET from eddy covariance measurements versus the sum of E from micrometeorological data and T from sap flow measurement is shown in the Fig. 6a. The partitioning of ET shows a good consistency compared to the total flux with a coefficient of determination equal to 0.94 and a root mean square error equal to 4.36 mm. During the dry years (2013 and 2015), maximum of monthly ET is around 50 mm. Monthly E represents a large fraction of ET, reaching 65% and 78% during August and September of 2013, respectively (López-Olivari et al., 2016; Roupsard et al., 2006). This behavior can be explained by the simultaneous rise of soil surface water content (due to the large number of small rain events) as well as evaporative demand associated to a high fraction of bare soil (0.93) at the stand scale in our site. Lower values of evaporation are recorded on account of the low amount of rainfall during the summer of 2014. During this wet period, T increases and dominates ET. The contribution of the transpiration rate is about 97.4% to the whole flux in the December of 2014.

The daily partitioning of the water fluxes varies enormously. The coefficient of determination of the daily scatter plot between ET and E + T (Fig. 6d) is about 0.64. During the summer of 2013 and the fall of 2014, the evaporation is the main part of the whole flux, especially during the two to three days following rainfall. Although evaporation reaches 70% of the whole flux (about 1.3 mm) on the day following the rain event of June 5, 2015, the daily transpiration peak occurs 6 days later.

As a first guess of the evapotranspiration and its components, the total Flux ET is evaluated through three means: one from measured flux, one obtained from the Bowen ratio correction method, and the other one from the residual method (see Section 2.2.2). Three estimates of soil evaporation (Merlin, Song and FAO) are applied (see Section 2.4). For the transpiration, the uncertainty estimates are derived from the two *SWA* calculations and the two upscaling methods (i.e., the average and the similar allometry methods) (see Section 2.3.1). The ranges of values between the minimum and the maximum of ET and its components from different methods are shown in the Fig. 7 as shaded area. The magnitude of ET varies largely especially during rainfall events. The largest shaded area for the soil evaporation occurs during the first evaporation stage and it is reduced during the second stage. The maximum ranges of transpiration are recorded during the wet year, i.e. in 2014. During dry years, the canopy decreases its transpiration by half roughly.

3.3. Analysis of evapotranspiration components and detection of soil and plant water stresses using different parameters

3.3.1. Transpiration and plant water stress

To study the year-to-year variability of the sap flow and the factors governing its dynamic at different scales, Fig. 8 shows the mean between 11h and 13h (local solar time), the range of the global incoming radiation, the *VPD*, and the sap flow. This temporal window is chosen because it corresponds to the maximum of incoming global solar radiation. The *PAW* varies markedly over the years (Fig. 8). It reaches

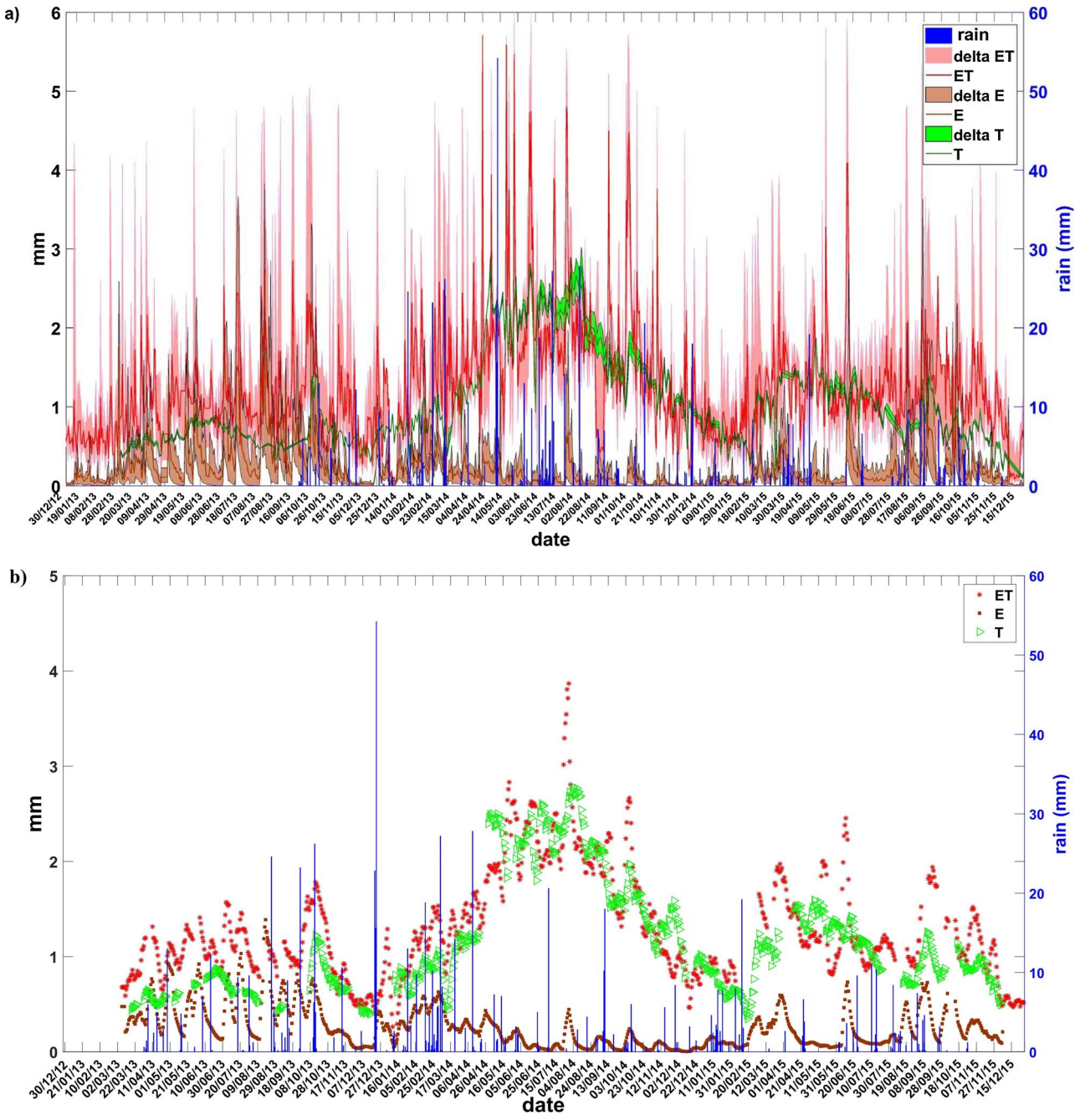

Fig. 7. The temporal evolution of evapotranspiration from eddy covariance (ET), the modeled evaporation based on*SWC* measurements (E) using the Merlin model and the transpiration from sap flow (T) during 2013, 2014 and 2015: a) daily mean with their corresponding uncertainty as shaded area; b) the moving average for a 7-day period.

100% and over (saturation) during the wet year, but usually about 40% during the dry years. It decreases rapidly following rainfall, especially during summer. Simultaneously, the sap flow reflects faithfully this year-to-year variability of the rainfall distribution. During the wet period, the sap flow is about twice those of 2013 and 2015 with a maximum of $2.5\,l\,h^{-1}\,dm^{-2}$. The standard deviation is higher during wet periods. The two minima of the sap flow over the three years of the study (near zero) are recorded during the dry periods, and they correspond not only to the minimum of the plant available water, but also to the minimum of *VPD* and of global radiation.

The observations reported in the literature suggest that, the daily fluctuations of sap flow are governed by the environmental conditions and its amplitude by the soil water content. Because our data are recorded under very contrasting climatic conditions, we select two pairs of days under the same climatic conditions and evaluate the effects of diurnal variations in meteorological conditions on daily dynamics of sap flow. We choose two days with a high water stress (the PAW of July 1, 2015 is about 33.37% and the *PAW* July 15, 2015 is about 32.68%) and two days with a moderate water stress (the *PAW* of August 9, 2014 is about 48.54% and the *PAW* of August 25, 2014 is about 41.7%). The daily course of sap flow, *VPD* and *Rg* follow a unimodal curve (Fig. 9). The irradiation and the *VPD* are found to explain sap flow fluctuations. The sap flow is null at night, increases sharply between 6 AM (local solar time) and 10 AM with a rise of global radiation ($950\,W\,m^{-2}$). The stomatal closure is visible at 10 AM for the four days as an evidence of plant water stress. The sap flow reaches its maximum and remained high at high *VPD* (420 Pa) till 2 PM, and diminishes gradually following the decrease of *VPD*. The maximum of global radiation occurs approximately at the same time as the maximum sap flow at 11 AM. The peak of *VPD* is observed later at 2 PM. The plant is subject to the same

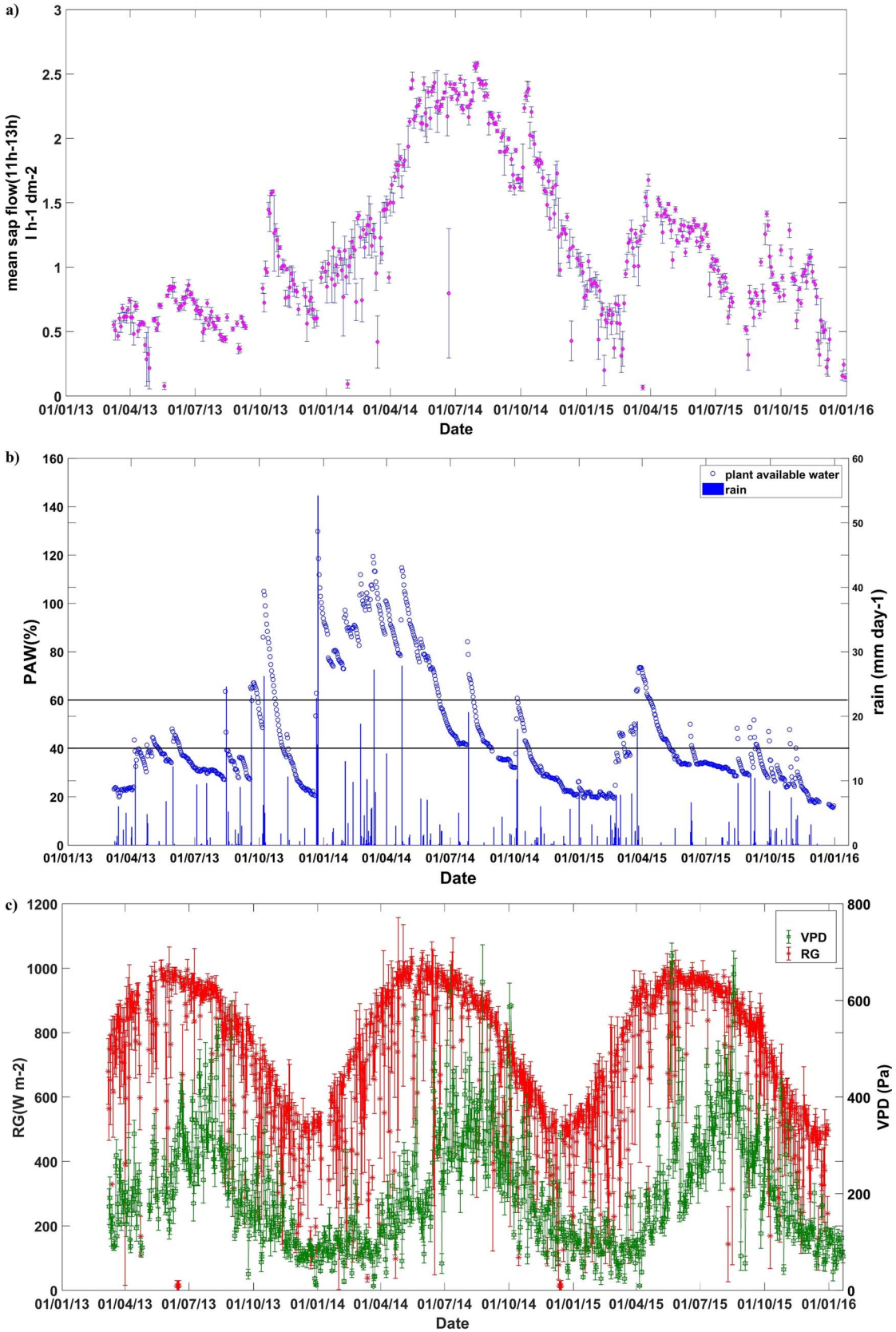

Fig. 8. (a) Dynamics of daily mean between 11h and 13h and the range of sap flow of the 8 sensors, (b) the plant available water (*PAW*) for the top 40 cm of soil, rain, (c) vapor pressure deficit (*VPD*) and global radiation (*Rg*) over the study period.

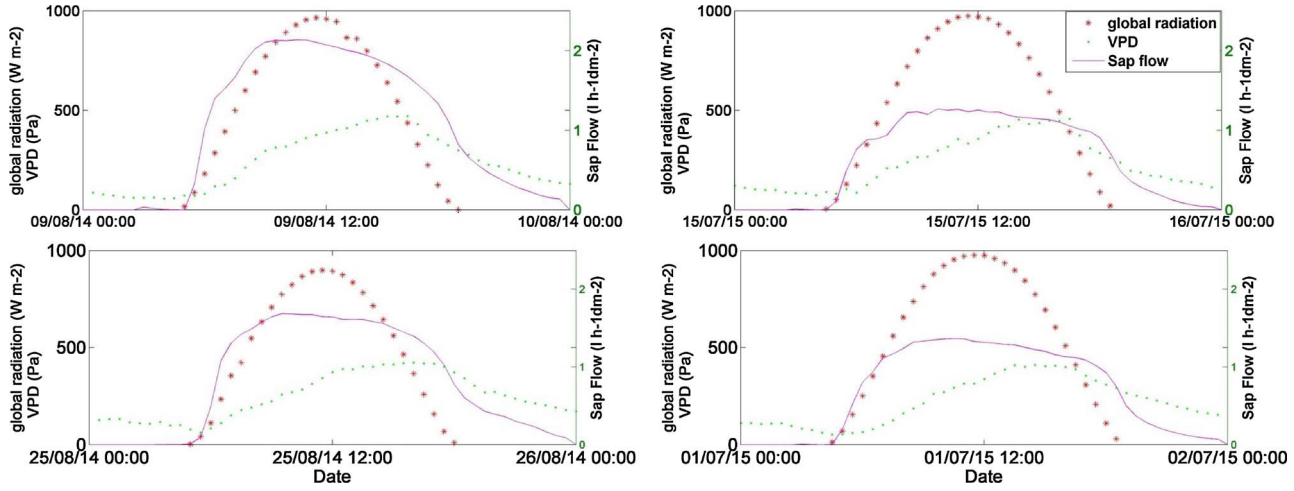

Fig. 9. Plots of half-hourly evolution of relative sap flow, vapor pressure deficit (*VPD*) and solar radiation on two typical days with moderate water stress, and two typical days with high soil water stress under the same meteorological conditions and the same LAI. Note that the *PAW* (the plant available water) on August 25, 2014 is 41.7%; the *PAW* on July 1, 2015 is 33.37%; the *PAW* on August 9, 2014 is 48.54%; the *PAW* on July 15, 2014 is 32.68%.

atmospheric conditions, but different water soil contents. The sap flow decreases from 1.68 l h^{-1} dm-^{2} to 1.3 l h^{-1} dm^{-2} on July 1, 2015. Similarly, it declines from 2.13 l h^{-1} dm^{-2} on August 9, 2014 to 1.26 l h^{-1} dm^{-2}.

Since the plant responds to both atmospheric conditions and soil water stress, we check the potential of remote sensing indices to detect the plant response to such water deficit or high atmospheric demand. Besides, we study the consistency between the vegetation stress index IS_v and the plant available water (Fig. 10). On June 15, 2015, the *PAW* remains under 40% and the plant was under high water stress. At that time, IS_v increases from 0.0038 to 0.0066 while the stress index *ITP* increases from 0.56 to 0.89. Similarly, in the same period of 2013, *ITP* is about 0.9, and IS_v is highly variable and ranges from 0.0031 to 0.008.

Once water stress is detected, a good estimate of the plant water use and a better comprehension of the hydrological functioning of the plant are needed. To quantify the plant water use, a scaling of sap flow measurements from individual trees give an estimation of the transpiration of the orchard from the sap flow measurements in individual trees (Fig. 7). Fig. 7 shows that the transpiration rates are low in 2013, high in 2014 and intermediate in 2015, which reflects the total amount of precipitation falling for each year. Daily means of transpiration did not exceed 3 mm day-1 from sap flow estimates as observed by Ramos and Santos (2009) for a dry-farming olive trees with 12 by 12 m spacing in southern Portugal. In the literature, such daily rates of transpiration are reported by David et al. (2007) for Mediterranean evergreen oaks. In an irrigated olive tree orchard in southern Italy, daily values of transpiration from 2 to 3 mm day-1 are also reported by Cammalleri et al. (2013).

Seasonal differences in transpiration are marked (Fig. 11). It ranges from 23.71 mm in the spring of 2013 to 106.83 mm in the wet summer of 2014.

3.3.2. Evaporation

For such a sparse cover, the bare soil represents a large contributing area. Soil evaporation is simulated over the study period using micrometeorological data and the SWC recorded in situ using Eqs (15) and (16). In this section, we study the soil evaporation and its response to a rain event. At the dry-down scale, we distinguish two stages of evaporation. We estimate the time between the rainfall and the transition from the climate controlled stage to the soil moisture controlled stage, through several parameters: the soil controlled evaporative index (IS_s), soil moisture and albedo as proposed by Amano and Salvucci (1999).

Fig. 7 shows the daily evaporation derived from the Merlin model based on the measured top soil water content. Over the three years of the experiment, we observe high evaporation values in 2013 and 2015 which are two dry years. During those years, rainfall is less significant but more frequent and occurs in the spring and the summer of 2013 and in the autumn of 2015. Daily E reaches 3 mm day^{-1} after a total amount of 30 mm of rain on August 2013. Even though the year of 2014 is characterized by major precipitation events especially in winter, E did not exceed 1 mm day^{-1}.

Albedo time series confirm that the surface temperature variations are due to deficit in soil water content. If we select pure dry downs (i.e. with no small amount of rainfall) (Fig. 12), we could observe that, after the rainfall, the curve can be divided into an initial sharp drop in volumetric water content and, some days after, a decrease in the evaporation rate resulted in a slope change (second stage). This shape corresponds closely to the two distinct stages of evaporation: the climate controlled and the soil moisture controlled stages. The time lag between the rain and the beginning of second stage (t_d) is between 1 and 3 days in this sandy soil. It coincides with an increase of albedo and of IS_s. Moreover, the selected rain event on December 23, 2013 corresponds to a total amount of 77 mm (Fig. 12 a). Fig. 12 shows the fast response of albedo, which increases from 0.22 to 0.35 four days after the rain. During the first stage of evaporation, IS_s is about 0.0066. When a small amount of precipitation falls on September 8, 2015 with a total amount of 13 mm, albedo increases from 0.3 to 0.34 and IS_s increases from 0.006 to 0.015. On October 7, 2013, a drop in the soil water content from 16 to 9% is concomitant with an increase in IS_s from 0.0033 to 0.015 and in albedo from 0.27 to 0.35. Similarly, after the rainfall of March 13, 2014, IS_s increases from 0.010 to 0.017 and albedo increases from 0.18 to 0.31. In all of those rain events, remote sensing variables are relevant for detecting the second stage of evaporation and are characterized by similar trends. However, this behavior is less noticeable after the rain event on April 23, 2014.

4. Discussion

The partitioning of the evapotranspiration is studied over three continuous years, which are characterized by a high year-to-year variability of the temporal distribution of rainfall. Due to an experimental protocol adapted to the very low vegetation fraction cover of the olive yard, this study provides a quantitative and qualitative analysis of the partitioning between the soil evaporation and the plant transpiration at different time scales, from the year-to-year variability down to the scale of a rain event.

The three contrasting years allow us to explore a large variety of drought level combinations as well as their effects on transpiration rates

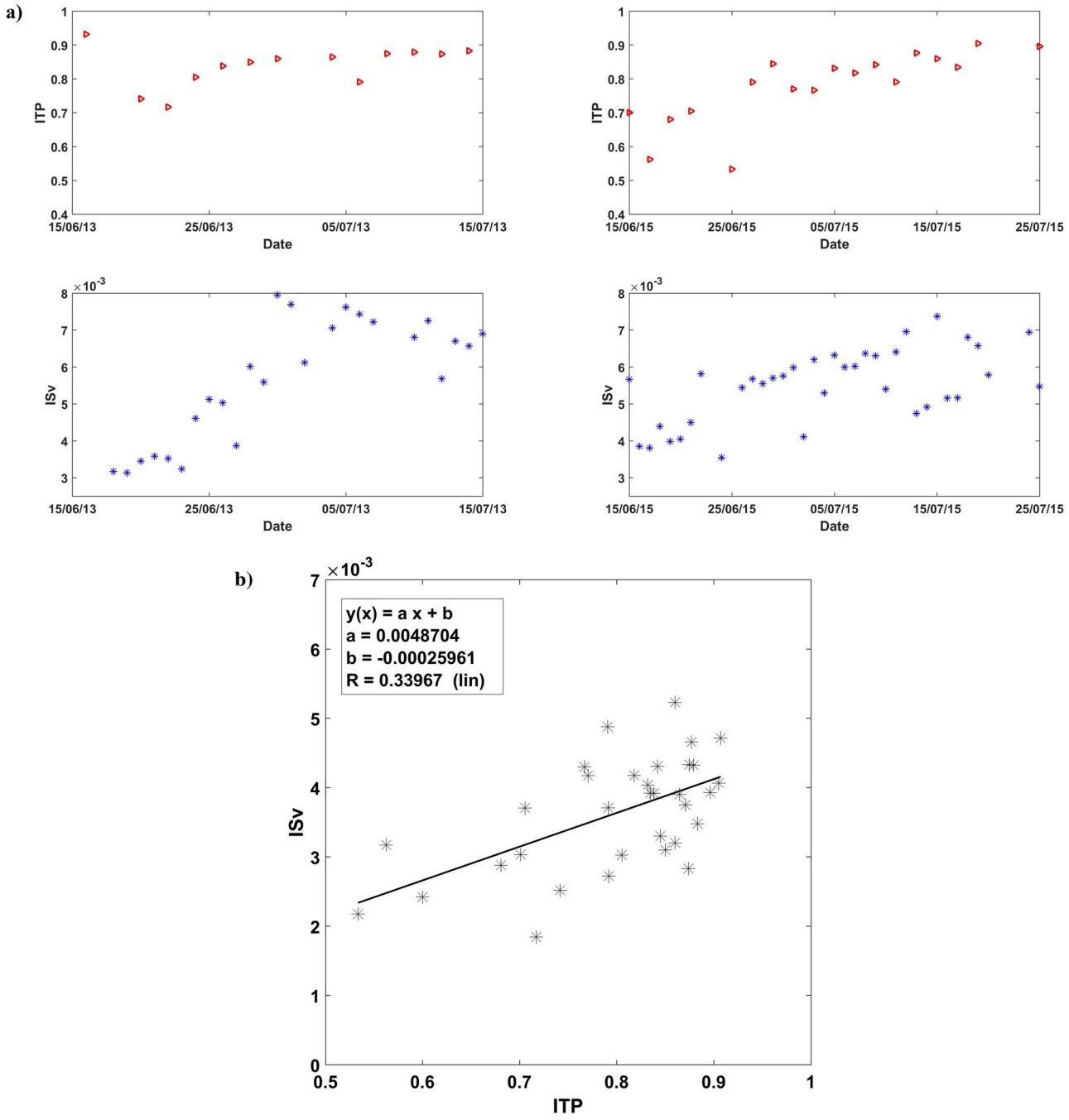

Fig. 10. (a) The mean of *ITP* (the potential transpiration indicator) and *ISv* (the vegetation stress indicator) between 11h and 13h after the rainfall event of June 1, 2013 and June 9, 2015 respectively; (b) the scatterplot between *ITP* and *ISv*. R is the coefficient of determination.

and evapotranspiration partitioning. Our study reveals a ratio T/ET ranging from 97% during wet periods to 4% during dry periods which can be explained by the seasonal rainfall intensity distribution. Even though 2013 and 2015 were dry years, there is a significant amount of small rainfall events during seasons with high climatic demand, which explains the large amount of E in those years compared to T: most of the rain is quickly returned to the atmosphere. During the wettest year 2014, however, rain falls less frequently but mostly in winter, when the climatic demand is low, and with large amounts which can penetrate the soil and refill the deeper horizons (Fig. 7). These results are within expected ranges of variability compared to those obtained over other olive orchards. For instance, Rousseaux et al. (2009) estimate that the transpiration contributed by 75% to the orchard ET over a drip-irrigated olive orchard with a fraction cover equal to 23%. Villalobos et al. (2000) investigate the evapotranspiration and its components over a drip irrigated olive orchard with a fraction cover of about 40% and a tree density of 277 tree ha^{-1}. The daily ratio T/ET, when the soil is dry, is about 76%. In our study, while having a fraction cover of 7% and a tree density of 25 tree ha^{-1}, when the annual rainfall is reduced by 43% from 2014 to 2015, the annual transpiration decreases by 20%. The year-to-year variation of transpiration is strongly correlated with the amount of the rainfall. This observation is consistent with the results obtained by Limousin et al. (2009). They show that a decrease of 29% of the rainfall lead to a decline of the annual transpiration by 23% using a 4-year throughfall exclusion experiment over Quercus ilex forest in a Mediterranean climate zone. However, our results are difficult to compare to previous works conducted on olive orchards because of their specific properties in terms of row spacing, climate, soil texture

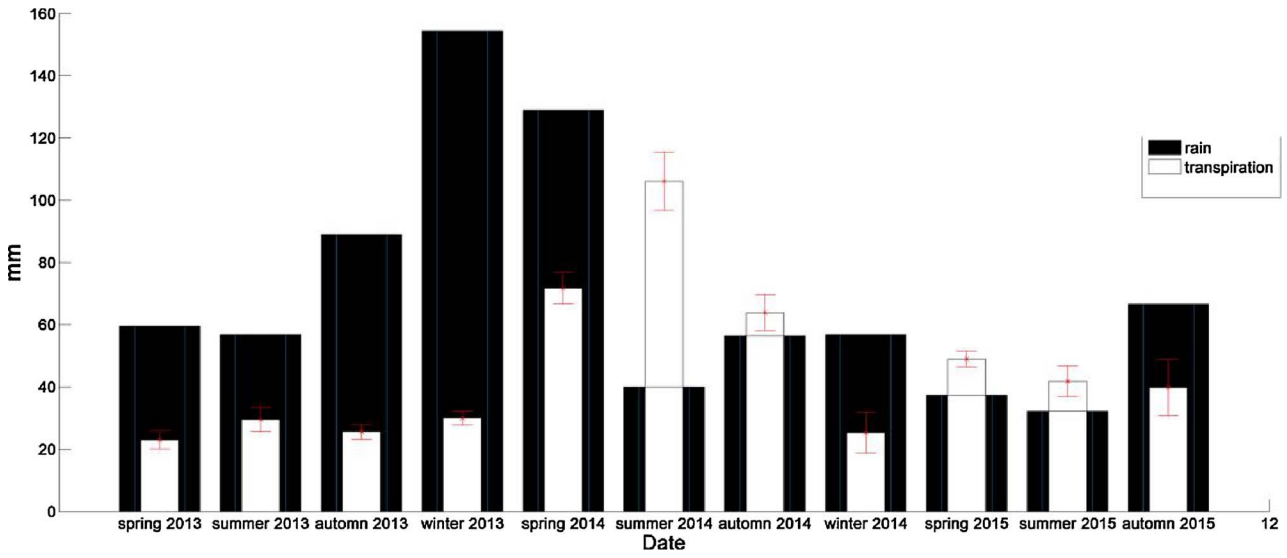

Fig. 11. Seasonal precipitation and transpiration from 2013 to 2015; the vertical red line represents the standard deviation of the transpiration.

and interest in irrigated sites (Charfi Masmoudi et al., 2011; Moreno et al., 1996; Santos et al., 2012; Tognetti et al., 2004).

To avoid any inconsistency in the partitioning due to the different methods used in this analysis of ET, we evaluate the quality of the dataset acquired using the eddy covariance technique through the energy balance closure. There is a small lack of energy balance closure at the orchard. Usually, the low measurments frequency does not allow to capture all eddies (Foken, 2008) and the available energy Rn-G is higher than the sum of the turbulent heat fluxes H + LE. This is not observed here. Nevertheless, the absolute difference between available energy and the sum of the turbulent fluxes remains consistent with previous works performed in many of the FLUXNET eddy covariance sites. In Wilson et al. (2002), the slopes evaluated over twenty-two sites and along fifty years range from 0.53 to 0.99, the intercepts (from -32.9 to 36.9 W m^{-2}) and the mean coefficients of determination (from 0.64 to 0.96). Several studies report a lack of energy balance closure using the eddy covariance method over olive orchards. For example, Er-Raki et al. (2008) report an imbalance ranging between 8 and 10% within the flood-irrigated Agdal olive orchard, located in Morocco. However, Villalobos et al. (2000) show for drip-irrigated olive orchards a good energy balance closure with a slope equal to 0.88, in addition to an intercept equal to 5.9 W m^{-2}.

Once the quality of the evapotranspiration dataset is checked, the most difficult step in using the other techniques is the scaling up to the orchard scale because of the specific and contrasted spatial scales of each of these methods. To estimate transpiration, we choose to install the sap flow sensors into four sampled trees. We consider this sample adequate on account of the homogenous tree size, row spacing and the absence of intercropping. The trees are near the eddy covariance mast and are part of the area contributing to the whole flux. The sensor position is important because the conducting system properties (uniformity of the sapwood area, conductivity…) vary according to the position (Kume et al., 2012; Lu et al., 2000; Oren et al., 1998). For the purpose of getting a representative measurements of the sap flow, we have to take into account this heterogeneity of the sapwood area and the intra-tree variability. At orchard scale, we use a method based on the trunk circumference (Vertessy et al., 1995) in order to scale-up sap flow density attributed to each tree of the sample to transpiration rate per unit of area. Several studies focus on the relationship between tree allometric measurements (circumference, trunk diameter, projected crown area…) and transpiration (Barbour et al., 2004; Kostner et al., 1996; Oren et al., 1996). In this study, scaling of the sap flow measurements to the tree transpiration require an estimation of the sapwood area of each sampled tree. This variable is a strong scaling factor, difficult to estimate and can lead to major errors (Kumagai et al., 2005) especially when averaged to the stand level (Nadezhdina et al., 2002). A sample of 25 trees for which we measure the trunk circumference, is considered as representative of the allometric variability of the orchard. Granier (1987) find that the transpiration per unit of conductive sapwood area is approximately constant between the trees and thus, in a homogenous orchard, four trees are adequate (Smith and Allen, 1996). In our study, contrarily to Williams et al. (2004), the transpiration rate with the sap flow method reaches but does not exceed the evapotranspiration rate derived from eddy covariance method, when the soil is dry. In Williams et al. (2004), the scaling of the transpiration to the evapotranspiration was necessary.

Another potential source of uncertainties is the change of temporal scale from hourly sap flow measurement to year-to-year estimations of transpiration rates. Indeed, in such environment, surrounding air temperature could generate noise in the sap flow measurements with the heat balance method. Even though the insulation cover is adequate to avoid the night offset and the morning peak, it seems to be insufficient (Lu et al., 2004) to overcome the natural gradients. To apply the temperature correction (see “materials and methods section”), we assume that the previous and the next day have similar weather conditions which probably is not always true. The gap-filling method is also based on meteorological variables, but meteorological conditions can be subject to rapid changes from one day to the next. In spite of these uncertainties, it is possible to estimate fairly accurately the transpiration of the day “off” using the gap-filling method based on the reference evapotranspiration. Moreover, the monthly results of the ET partitioning (Fig. 6) demonstrate a good fit between the sum of the evaporation and the transpiration, and that of the evapotranspiration, as a proof of the robustness of the approach.

Monthly transpiration rates range from 3 mm in September of 2013 to 74 mm in August of 2014 which coincide with maximum solar irradiance and net radiation. This estimates fall within the range of values measured under semi-arid conditions: (Santos et al., 2012) estimate the transpiration of dry-farming olive orchard of about 27.3 mm from August 4 to August 17 and 44 mm from August 18 to September 9. The high transpiration rates recorded during the driest summer period (i.e. in 2014) reveals a slight relationship with rainfall events (Fig. 11) which acts in contradiction with previous works (Zhang et al., 2015; Zhao and Liu, 2010). The large amount of precipitation falling during the autumn and the winter of 2014 seems to be sufficient to supply the stock of water available to the plant in summer. A similar observation is

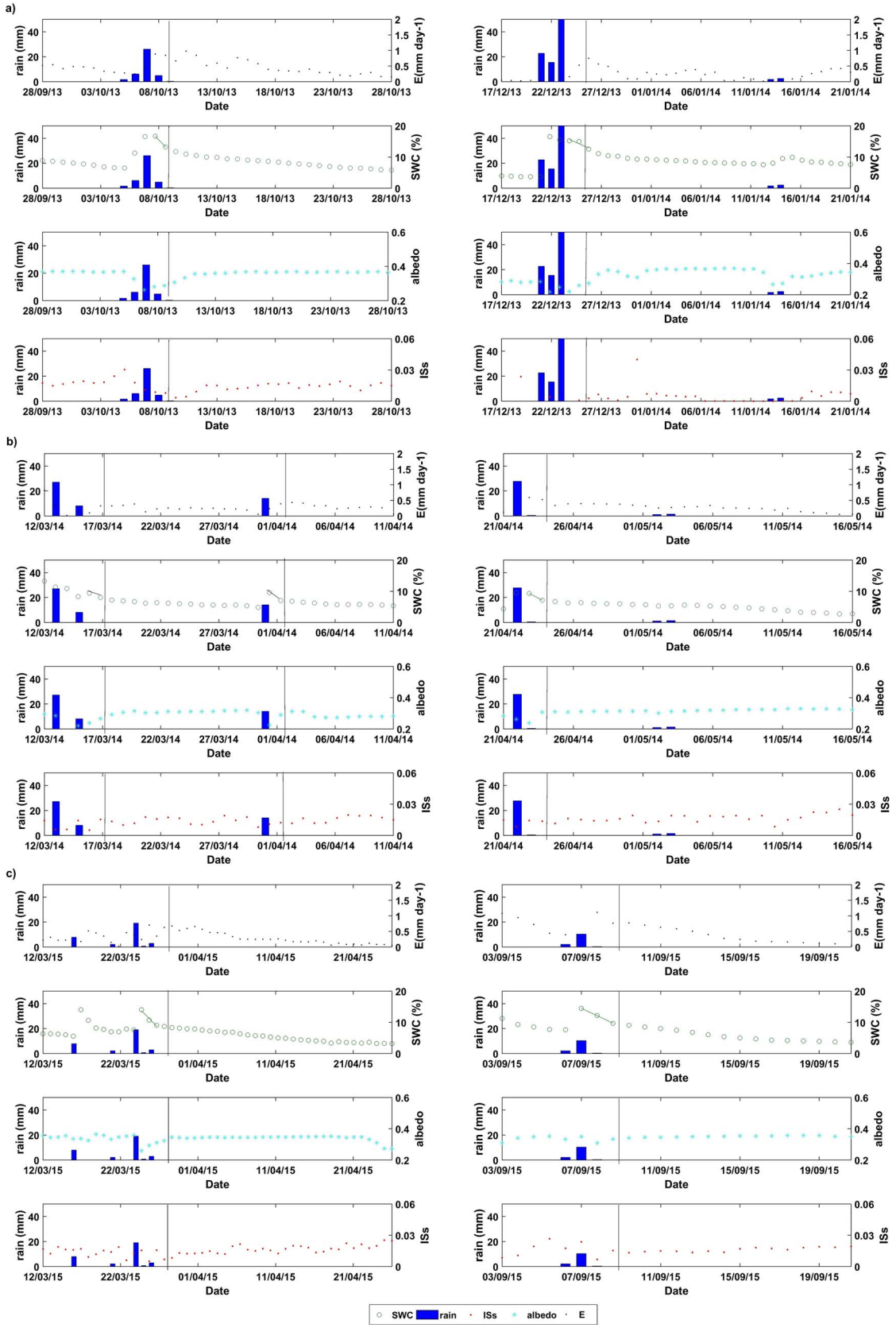

Fig. 12. Daily evaporation, volumetric water content albedo and IS_s for specified days after rainfall at different time of the period of study (a) 2013, b) 2014, c) 2015). The vertical black line shows the limit between the two stages of evaporation: the atmosphere limited stage and the soil limited. *SWC* is the volumetric humidity; E is the soil evaporation; IS_s is the soil controlled evaporative index. The bars represent the daily rainfall.

Table 1
The seasonal water balance: total rain versus the sum of the total water storage evolution over the top meter of soil (ΔS) and the evapotranspiration (ET). Automn is: September-October-November. Winter is: December-January-February. Spring is: March-April-May. Summer is: June-July-August. Bold numbers refer to seasons when ΔS + ET exceed the rainfall.

	Cumulative sum rain	Cumulative sum (ΔS + ET)
Winter 2013	**29.8**	**52.3**
Spring 2013	**60**	**76.0**
Summer 2013	**56.8**	**77.0**
Autumn 2013	89	89.2
Winter 2014	154.2	112.8
Spring 2014	128.4	132.9
Summer 2014	**40.8**	**175.0**
Autumn 2014	**56.4**	**123.1**
Winter 2015	70.6	63.4
Spring 2015	**37.4**	**62.7**
Summer 2015	**32.2**	**99.7**
Autumn 2015	**66.6**	**143.8**

reported by Masmoudi-Charfi (2013) which conclude that soil water use in an olive orchard is correlated with the previous rainy season. Therefore, the contribution of transpiration in evapotranspiration is dominant for the dry periods in 2014, whereas the rainfall and the soil water storage at 1 m did not supply transpiration rates suggesting soil water extraction from the soil below 1 m by deep roots. Table 1 shows that, during wet periods, the tree extracts water from the soil top meter and thus the top meter soil water balance is mostly closed. However, during dry periods (in bold in the Table 1), the sum of the soil water storage at the top meter of soil and the evapotranspiration exceeds the amount of rainfall because the tree uses its deep roots to extract water from deeper horizons. This ability of deep root water extraction by trees under water deficit is reported by Moreno et al. (1996) for an olive orchard in Spain. Overall, there is a lack of information in the literature on root distribution on account of the difficulty of its measurement. Consequently, it may limit the accuracy of the plant available water estimate. However, several works report high rooting depth under water deficit conditions, reaching sometimes 12 m for trees in semi-arid areas (Brito et al., 2015). No study dedicated to a rainfed olive orchard is found. But, the 20 m by 20 m spacing allows the tree to explore a large volume of soil. The Fig. 4 shows a high root density at the surface near the trunk and in deeper soil layers, far away from the trunk, as discussed by Fernández et al. (1991).

In our analysis at the event scale, the response of the transpiration to a rain event shows a lag that is extremely variable. No single factor can explain the time lag required to an increase of sap flow following water supply. The length of the drought period preceding the event, the precipitation amount, the soil water content and the plant water status before the event should be explored simultaneously to further understand this response (Fig. 13). After the rain event of June 5, 2015, the transpiration increases from 0.3 mm to 0.9 mm and represents 62% of the whole flux after the first four days following the rain. After a long dry down, when the rain of June 9, 2015 falls, the transpiration response is slow and reaches its highest value after six days (1.52 mm). However, when the soil is already wet, the small rain event of April 13, 2014 which occurs 13 days after a larger one, boosts rapidly the transpiration which reaches 75% of the evapotranspiration two days after the rain. On the other hand, the time lag seems to be longer when rain is falling after a long period of drought and the ratio of transpiration to the potential transpiration (T/T_p) is close to 0 for days such as June 9, 2015 and April 26, 2015. Within that condition of high soil water deficit, the first rain event allows mostly the water recharge of plant tissues, before causing a boost of transpiration. When the soil is dry at the end of long dry downs, the transpiration is equal to the evapotranspiration.

Beside soil water availability, our study shows that the global radiation and the *VPD* affects the day-to-day dynamics of sap flow, as reported by Tognetti et al. (2004) for olive trees. According to the Fig. 9, the increase of incoming radiation in the morning causes a rise of sap flow density associated to an activation of photosynthetic processes (Wullschleger et al., 2001). However, after 10 AM, sap flow declines gradually. This response is more pronounced under soil water deficit conditions probably due to a more severe reduction of stomatal conductance (i.e., July 1, 2015 and July 15, 2015). As described before in the literature (Xu et al., 2010), by reducing stomatal conductance, plants can adjust their water loss in case of high soil water deficit. However, even in case of low soil water content, sap flow density is maintained because of high values in VPD recorded in the afternoon. This is consistent with Fernández et al. (1997) and Oren et al. (1999), which show that photosynthesis and plant growth are probably maintained through using water available in the deeper layers. An increase of Water Use Efficiency (WUE), defined as the ratio between yield and irrigation, is previously reported for olive trees in the case of soil water deficit (Iniesta et al., 2008; Romero et al., 2002; Tognetti et al., 2006; Wahbi et al., 2005). We should note that WUE is usually calculated as a function of water supply by irrigation and at annual scale. Authors rarely use the transpiration rate to define WUE, even though transpiration is the main physiological indicator, because of the difficulty of its measurement.

In order to check, with independent measurements, the consistency of the plant water stress and the remote sensing indicator IS_v, a similar analysis to what has been done for the determination of stage two evaporation can be also carried out for the transpiration in water limited conditions. According to the Fig. 10, IS_v increases significantly with an increase of the *ITP*. The switch from well-watered to water- stressed conditions can be related to an increase in the surface temperature. Under high water stress, Diaz-Espejo et al. (2007) notice the increase of olive leaf temperature after the stomatal closure. Within the same context, Sepulcre-Cantó et al. (2006) evaluate the difference of the leaf surface temperature values between a well-irrigated olive tree and a water-stressed tree. This difference could reach 4° K. In our case, it is less pronounced due to the poor calibration of the thermal sensor and more probably to the complex canopy structure of sparse trees, causing a high contribution of soil in the signal.

5. Conclusions

Continuous energy and flux partitioning measurements during 3 years over a sparse dry-farming olive orchard provides information about the evapotranspiration and its components and thus the interplay between the water use of the olive tree and the water loss from the soil. This orchard represents one of the widespread cultivation practices in Tunisia and in the Mediterranean basin. Inter-annual variability in evapotranspiration is as high as that in rainfall in these semi-arid systems. The soil evaporation can be computed from the SWC of the top soil layer (0–5 cm). Although it is controlled by atmospheric conditions during its first stage relatively short (2–3 days) and reacts at the potential rate, it is still dominated by soil properties and decreases gradually during its second stage. The soil water loss is important (78%) in such area. The tree transpiration was mainly a function of deeper soil water content (20–40 cm: zone of maximum of rooting). Due to the capacity of its root system to extract water from deep layers, the tree reduces its transpiration to fit water and atmospheric stress by the stomatal closure and succeeds in maintaining a constant rate of transpiration during dry periods. The water use of the tree is the major component (98%) when the plant available water is high and the top soil layer is dry. Therefore, we recommended the use of the combination of the eddy covariance for the evapotranspiration, the sap flow for the transpiration and the model for the evaporation, as described below, to study the whole flux and its components within this difficult environment. Ultimately, it will be very interesting to apply a SVAT model to represent the impact of canopy structure on radiative and

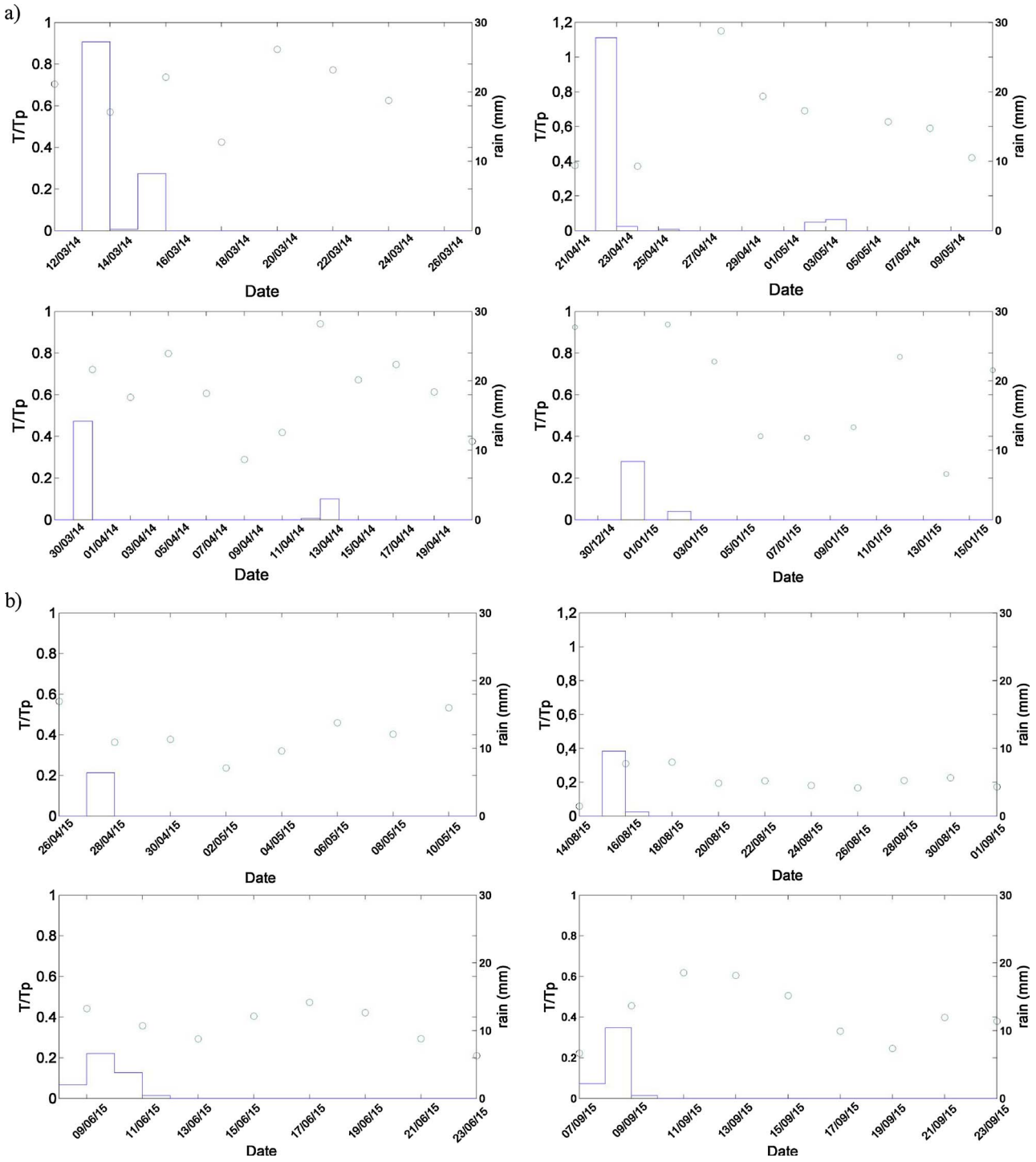

Fig. 13. The dynamics of the ratio of the daily transpiration to the potential transpiration (T/T_p). Bars are the rain.

turbulent exchanges and the ecophysiology (stomatal processes, hydraulic resistance, root extraction ...) as well as to test more prolonged drought scenarios in the future. The method of partitioning cited by Anderson et al. (2017) will be tested on our dataset. Our data are available online: Chebbi (2017).

Acknowledgements

This work was permitted with the collaboration of the IO (l'institut de l'olivier). We also thank the Tunisian Ministry of higher education and scientific Research for granting students involved in this study. Financial support from the MISTRALS/SICMED program for the ReSAMEd project, from the CNES/TOSCA program for the EVA2IRT project, from the ORFEO/CNES Program for Pléiades images (© CNES 2012, Distribution Airbus DS, all rights reserved) and from the ANR/TRANSMED program for the AMETHYST project (ANR-12-TMED-0006-01) are gratefully acknowledge, as well as the mobility support from PHC Maghreb program (N° 32592VE/PHC 14 MAG 22).

Appendix A. Supplementary data

Supplementary material related to this article can be found, in the

online version, at doi:https://doi.org/10.1016/j.agrformet.2018.02.020.

References

Allen, R.G., Pereira, L.S., Howell, T.A., Jensen, M.E., 2011. Evapotranspiration information reporting: I. Factors governing measurement accuracy. Agric. Water Manag. 98, 899–920. http://dx.doi.org/10.1016/j.agwat.2010.12.015.

Allen, R.G., Pereira, L.S., Raes, D., Smith, M., 1998. Crop evapotranspiration -guidelines for computing crop water requirements. FAO Irrigation and Drainage Paper 56. pp. 300.

Amano, E., Salvucci, G.D., 1999. Detection and use of three signatures of soil-limited evaporation. Remote Sens. Environ. 67, 108–122. http://dx.doi.org/10.1016/S0034-4257(98)00076-5.

Anderson, R.G., Alfieri, J.G., Tirado-Corbalá, R., Gartung, J., McKee, L.G., Prueger, J.H., Wang, D., Ayars, J.E., Kustas, W.P., 2017. Assessing FAO-56 dual crop coefficients using eddy covariance flux partitioning. Agric. Water Manag. 179, 92–102. http://dx.doi.org/10.1016/j.agwat.2016.07.027.

Anderson, R.G., Wang, D., 2014. Energy budget closure observed in paired eddy covariance towers with increased and continuous daily turbulence. Agric. For. Meteorol. 184, 204–209. http://dx.doi.org/10.1016/J.AGRFORMET.2013.09.012.

Arora, V., 2002. Modeling vegetation as a dynamic component in soil-vegetation-atmosphere transfer schemes and hydrological models. Rev. Geophys. 40, 1006. http://dx.doi.org/10.1029/2001RG000103.

Bailey, B., Montero, J., Biel, C., Wilkinson, D., Anton, A., Jolliet, O., 1993. Transpiration of Ficus benjamina: comparison of measurements with predictions of the Penman-Monteith model and a simplified version. Agric. For. Meteorol. 65, 229–243. http://dx.doi.org/10.1016/0168-1923(93)90006-4.

Baldocchi, D.D., Hincks, B.B., Meyers, T.P., 1988. Measuring biosphere-atmosphere exchanges of biologically related gases with micrometeorological methods. Ecology 69, 1331–1340. http://dx.doi.org/10.2307/1941631.

Baldocchi, D.D., Xu, L., Kiang, N., 2004. How plant functional-type, weather, seasonal drought, and soil physical properties alter water and energy fluxes of an oak-grass savanna and an annual grassland. Agric. For. Meteorol. 123, 13–39. http://dx.doi.org/10.1016/j.agrformet.2003.11.006.

Barbour, M.M., Hunt, J.E., Walcroft, A.S., Rogers, G.N.D., McSeveny, T.M., Whitehead, D., 2004. Components of ecosystem evaporation in a temperate coniferous rainforest, with canopy transpiration scaled using sapwood density. New Phytol. 165, 549–558. http://dx.doi.org/10.1111/j.1469-8137.2004.01257.x.

Ben Ahmed, C., Rouina, B., Boukhris, M., 2007. Effects of water deficit on olive trees cv. Chemlali under field conditions in arid region in Tunisia. Sci. Hortic. (Amsterdam). 113, 267–277. http://dx.doi.org/10.1016/j.scienta.2007.03.020.

Ben Aissa, I., Bouarfa, S., Perrier, A., 2009. Utilisation de la mesure thermique du flux de eve pour l evaluation de la transpiration d'un palmier dattier. pp. 12.

Biogeochemical Integration | Services / REddyProcWebGapFilling [WWW Document], 2011. URL https://www.bgcjena.mpg.de/bgi/index.php/Services/REddyProcWebGapFilling (Accessed 1 July 2017).

Boulet, G., Braud, I., Vauclin, M., 1997. Study of the mechanisms of evaporation under arid conditions using a detailed model of the soil–atmosphere continuum: application to the EFEDA I experiment. J. Hydrol. 193, 114–141. http://dx.doi.org/10.1016/S0022-1694(96)03148-4.

Boulet, G., Chehbouni, A., Braud, I., Vauclin, M., Haverkamp, R., Zammit, C., 2000. A simple water and energy balance model designed for regionalization and remote sensing data utilization. Agric. For. Meteorol. 105, 117–132. http://dx.doi.org/10.1016/S0168-1923(00)00184-2.

Boulet, G., Chehbouni, A., Gentine, P., Duchemin, B., Ezzahar, J., Hadria, R., 2007. Monitoring water stress using time series of observed to unstressed surface temperature difference. Agric. For. Meteorol. 146, 159–172. http://dx.doi.org/10.1016/j.agrformet.2007.05.012.

Boussadia, O., Mariem, F.Ben, Mechri, B., Boussetta, W., Braham, M., Hadj, S.B.El, 2008. Response to drought of two olive tree cultivars (cv Koroneki and Meski). Sci. Hortic. (Amsterdam) 116, 388–393. http://dx.doi.org/10.1016/j.scienta.2008.02.016.

Brito, P., Lorenzo, J.R., González-Rodríguez, Á.M., Morales, D., Wieser, G., Jiménez, M.S., 2015. Canopy transpiration of a semi arid Pinus canariensis forest at a treeline ecotone in two hydrologically contrasting years. Agric. For. Meteorol. 201, 120–127. http://dx.doi.org/10.1016/j.agrformet.2014.11.008.

Bustan, A., Dag, A., Yermiyahu, U., Erel, R., Presnov, E., Agam, N., Kool, D., Iwema, J., Zipori, I., Ben-Gal, A., 2015. Fruit load governs transpiration of olive trees. Tree Physiol. 36, 380–391. http://dx.doi.org/10.1093/treephys/tpv138.

Caldwell, M.M., Dawson, T.E., Richards, J.H., 1998. Hydraulic lift: consequences of water efflux from the roots of plants. Oecologia 113, 151–161. http://dx.doi.org/10.1007/s004420050363.

Calvet, J.-C., Gibelin, A.-L., Roujean, J.-L., Martin, E., Le Moigne, P., Douville, H., Noilhan, J., 2008. Past and future scenarios of the effect of carbon dioxide on plant growth and transpiration for three vegetation types of southwestern France. Atmos. Chem. Phys. Atmos. Chem. Phys. 8, 397–406.

Calvet, J.-C., Noilhan, J., Roujean, J.-L., Bessemoulin, P., Cabelguenne, M., Olioso, A., Wigneron, J.-P., 1998. An interactive vegetation SVAT model tested against data from six contrasting sites. Agric. For. Meteorol. 92, 73–95. http://dx.doi.org/10.1016/S0168-1923(98)00091-4.

Cammalleri, C., Rallo, G., Agnese, C., Ciraolo, G., Minacapilli, M., Provenzano, G., 2013. Combined use of eddy covariance and sap flow techniques for partition of ET fluxes and water stress assessment in an irrigated olive orchard. Agric. Water Manag. 120, 89–97. http://dx.doi.org/10.1016/j.agwat.2012.10.003.

Masmoudi, Charfi, C, Masmoudi, M, Abid-Karray, J, Mechlia, Ben, N., 2011. Sap flow measurements in young olive trees (Olea europaea L.) cv. Chétoui under Tunisian conditions. Sci. Hortic. (Amsterdam) 129, 520–527. http://dx.doi.org/10.1016/j.scienta.2011.05.030.

Chebbi, W., 2017. nasrallah flux database [WWW Document]. SEDOO OMP website. doi:DOI: 10.6096/MISTRALS-SICMED.1479.

Connor, D.J., Gómez-del-Campo, M., Rousseaux, M.C., Searles, P.S., 2014. Structure, management and productivity of hedgerow olive orchards: A review. Sci. Hortic. (Amsterdam) 169, 71–93. http://dx.doi.org/10.1016/j.scienta.2014.02.010.

David, T.S., Henriques, M.O., Kurz-Besson, C., Nunes, J., Valente, F., Vaz, M., Pereira, J.S., Siegwolf, R., Chaves, M.M., Gazarini, L.C., David, J.S., 2007. Water-use strategies in two co-occurring Mediterranean evergreen oaks: surviving the summer drought. Tree Physiol. 27, 793–803. http://dx.doi.org/10.1093/treephys/27.6.793.

Diaz-Espejo, A., Nicolás, E., Fernández, J.E., 2007. Seasonal evolution of diffusional limitations and photosynthetic capacity in olive under drought. Plant Cell Environ. 30, 922–933. http://dx.doi.org/10.1111/j.1365-3040.2007.001686.x.

Do, F., Rocheteau, A., 2002. Influence of natural temperature gradients on measurements of xylem sap flow with thermal dissipation probes. 2. advantages and calibration of a noncontinuous heating system. Tree Physiol. 22, 649–654.

Er-Raki, S., Chehbouni, A., Ezzahar, J., Khabba, S., Boulet, G., Hanich, L., Williams, D., 2009. Evapotranspiration partitioning from sap flow and eddy covariance techniques for olive orchards in semi-arid region. Acta Hortic. 201–208. http://dx.doi.org/10.17660/ActaHortic.2009.846.21.

Er-Raki, S., Chehbouni, A., Hoedjes, J.C.B., Ezzahar, J., Duchemin, B., Jacob, B., 2008. Improvement of FAO-56 method for olive orchards through sequential assimilation of thermal infrared-based estimates of ET. Agric. Water Manag. 95, 309–321. http://dx.doi.org/10.1016/J.AGWAT.2007.10.013.

Fernández, J.E., Moreno, F., 1999. Water use by the olive tree. J. Crop. Prod. 2, 101–162.

Fernández, J.E., Moreno, F., Cabrera, F., Arrue, J.L., Martín-Aranda, J., 1991. Drip irrigation, soil characteristics and the root distribution and root activity of olive trees. Plant Soil 133, 239–251. http://dx.doi.org/10.1007/BF00009196.

Fernández, J.E., Moreno, F., Girón, I.F., Blázquez, O.M., 1997. Stomatal control of water use in olive tree leaves. Plant Soil 190, 179–192. http://dx.doi.org/10.1023/A:1004293026973.

Foken, T., 2008. The energy balance closure problem: an overview. Ecol. Appl. 18, 1351–1367. http://dx.doi.org/10.1890/06-0922.1.

Gargouri, K., Rhouma, A., Sahnoun, A., Ghribi, M., Bentaher, H., Rouina, B.B., Ghrab, M., 2008. Assessment of the impact of climate change on olive growing in Tunisia using GIS tools. Options Méditerranéennes Ser. A.

Gebler, S., Hendricks Franssen, H.-J., Pütz, T., Post, H., Schmidt, M., Vereecken, H., 2015. Actual evapotranspiration and precipitation measured by lysimeters: a comparison with eddy covariance and tipping bucket. Hydrol. Earth Syst. Sci. 19, 2145–2161. http://dx.doi.org/10.5194/hess-19-2145-2015.

Gómez-Rico, A., Salvador, M.D., Moriana, A., Pérez, D., Olmedilla, N., Ribas, F., Fregapane, G., 2007. Influence of different irrigation strategies in a traditional Cornicabra cv. olive orchard on virgin olive oil composition and quality. Food Chem. 100, 568–578. http://dx.doi.org/10.1016/j.foodchem.2005.09.075.

Granier, A., 1987. Evaluation of transpiration in a Douglas-fir stand by means of sap flow measurements. Tree Physiol. 3, 309–320. http://dx.doi.org/10.1093/treephys/3.4.309.

Granier, A., 1985. Une nouvelle méthode pour la mesure du flux de sève brute dans le tronc des arbres. Ann. des Sci. For. 42, 193–200. http://dx.doi.org/10.1051/forest:19850204.

Horst, T.W., Weil, J.C., 1994. How far is far enough?: the fetch requirements for micrometeorological measurement of surface fluxes. J. Atmos. Ocean. Technol 11, 1018–1025. http://dx.doi.org/10.1175/1520-0426(1994)011&1018:HFIFET&2.0.CO;2.

Iniesta, F., Testi, L., Orgaz, F., Villalobos, F.J., 2008. The effects of regulated and continuous deficit irrigation on the water use, growth and yield of olive trees. Eur. J. Agron. 30, 258–265.

Jackson, D., Paglietti, L., Ribeiro, M., Karray, B., 2015. Tunisie: Analyse de la filière oléicole. Rome. .

Jackson, R.D., Idso, S.B., Reginato, R.J., Pinter, P.J., 1981. Canopy temperature as a crop water stress indicator. Water Resour. Res. 17, 1133–1138. http://dx.doi.org/10.1029/WR017i004p01133.

Kelliher, F.M., Köstner, B.M.M., Hollinger, D.Y., Byers, J.N., Hunt, J.E., McSeveny, T.M., Meserth, R., Weir, P.L., Schulze, E.D., 1992. Evaporation, xylem sap flow, and tree transpiration in a New Zealand broad-leaved forest. Agric. For. Meteorol. 62, 53–73. http://dx.doi.org/10.1016/0168-1923(92)90005-O.

Kölling, K., George, G.M., Künzli, R., Flütsch, P., Zeeman, S.C., 2015. A whole-plant chamber system for parallel gas exchange measurements of Arabidopsis and other herbaceous species. Plant Methods 11, 48. http://dx.doi.org/10.1186/s13007-015-0089-z.

Kool, D., Ben-Gal, A., Agam, N., Šimůnek, J., Heitman, J.L., Sauer, T.J., Lazarovitch, N., 2014. Spatial and diurnal below canopy evaporation in a desert vineyard: measurements and modeling. Water Resour. Res. 50, 7035–7049. http://dx.doi.org/10.1002/2014WR015409.

Kool, D., Kustas, W.P., Ben-Gal, A., Lazarovitch, N., Heitman, J.L., Sauer, T.J., Agam, N., 2016. Energy and evapotranspiration partitioning in a desert vineyard. Agric. For. Meteorol. 218, 277–287. http://dx.doi.org/10.1016/j.agrformet.2016.01.002.

Kostner, B., Biron, P., Siegwolf, R., Granier, A., 1996. Estimates of water vapor flux and canopy conductance of scots pine at the tree level utilizing different xylem sap flow methods. Theor. Appl. Climatol. 53, 105–113. http://dx.doi.org/10.1007/BF00866415.

Kuchment, L.S., Singh, V.P., 2009. Models of vertical energy and water transfer within the "soil-vegetation-atmosphere" system. Hydrological Systems Modeling - Volume I.

Eolss, oxford, pp. 349.
Kumagai, T., Nagasawa, H., Mabuchi, T., Ohsaki, S., Kubota, K., Kogi, K., Utsumi, Y., Koga, S., Otsuki, K., 2005. Sources of error in estimating stand transpiration using allometric relationships between stem diameter and sapwood area for Cryptomeria japonica and Chamaecyparis obtusa. For. Ecol. Manage. 206, 191–195. http://dx.doi.org/10.1016/j.foreco.2004.10.066.
Kume, T., Otsuki, K., Du, S., Yamanaka, N., Wang, Y.-L., Liu, G.-B., 2012. Spatial variation in sap flow velocity in semiarid region trees: its impact on stand-scale transpiration estimates. Hydrol. Process. 26, 1161–1168. http://dx.doi.org/10.1002/hyp.8205.
Lagouarde, J.-P., Ballans, H., Moreau, P., Guyon, D., Coraboeuf, D., 2000. Experimental study of brightness surface temperature angular variations of maritime pine (Pinus pinaster) stands. Remote Sens. Environ. 72, 17–34. http://dx.doi.org/10.1016/S0034-4257(99)00085-1.
Leuning, R., Gorsel, E., van, Massman, W.J., Issac, P.R., 2012. Reflections on the surface energy imbalance problem. Agric. For. Meteorol 156, 65–74. http://dx.doi.org/10.1016/J.AGRFORMET.2011.12.002.
Limousin, J.M., Rambal, S., Ourcival, J.M., Rocheteau, A., Joffre, R., Rodriguez-Cortina, R., 2009. Long-term transpiration change with rainfall decline in a Mediterranean Quercus ilex forest. Glob. Change Biol. 15, 2163–2175. http://dx.doi.org/10.1111/j.1365-2486.2009.01852.x.
López-Olivari, R., Ortega-Farías, S., Poblete-Echeverría, C., 2016. Partitioning of net radiation and evapotranspiration over a superintensive drip-irrigated olive orchard. Irrig. Sci. 34, 17–31. http://dx.doi.org/10.1007/s00271-015-0484-2.
Lu, P., Laurent, U., Zhao, P., 2004. Granier's thermal dissipation probe (TDP) method for measuring sap flow in trees: theory and practice. Acta Bot. Sin. 46, 631–646.
Lu, P., Müller, W.J., Chacko, E.K., 2000. Spatial variations in xylem sap flux density in the trunk of orchard-grown, mature mango trees under changing soil water conditions. Tree Physiol. 20, 683–692.
Masmoudi-Charfi, C., 2013. Growth of Young olive trees: water requirements in relation to canopy and root development. Am. J. Plant Sci. 4, 1316–1344. http://dx.doi.org/10.4236/ajps.2013.47163.
Merlin, O., Al Bitar, A., Rivalland, V., Béziat, P., Ceschia, E., Dedieu, G., Merlin, O., Bitar, A.Al, Rivalland, V., Béziat, P., Ceschia, E., Dedieu, G., 2011. An analytical model of evaporation efficiency for unsaturated soil surfaces with an arbitrary thickness. J. Appl. Meteorol. Climatol. 50, 457–471. http://dx.doi.org/10.1175/2010JAMC2418.1.
Michiles, A.A., dos, S., Gielow, R., 2008. Above-ground thermal energy storage rates, trunk heat fluxes and surface energy balance in a central amazonian rainforest. Agric. For. Meteorol. 148, 917–930. http://dx.doi.org/10.1016/j.agrformet.2008.01.001.
Moreno, F., Fernandez, J.E., Clothier, B.E., Green, S.R., 1996. Transpiration and root water uptake by olive trees. Plant Soil 184, 85–96. http://dx.doi.org/10.1007/BF00029277.
Nadezhdina, N., Jan, C., Reinhart, C., 2002. Radial patterns of sap flow in woody stems of dominant and understory species: scaling errors associated with positioning of sensors. Tree Physiol. 22, 907–918.
Nicolas, E., Torrecillas, A., Ortuno, M.F., Domingo, M., Alarcon, J.J., 2005. Evaluation of transpiration in adult apricot trees from sap flow measurements. Agric. Water Manag. 72, 131–145. http://dx.doi.org/10.1016/J.AGWAT.2004.09.008.
Observatoire National de l'Agriculture [WWW Document], 2017. URL http://www.onagri.nat.tn/indicateurs (Accessed 10 October 2017).
Oren, R., Phillips, N., Katul, G., Ewers, B.E., Pataki, D.E., 1998. Scaling xylem sap flux and soil water balance and calculating variance: a method for partitioning water flux in forests. Ann. Des. Sci. For. 55, 191–216. http://dx.doi.org/10.1051/forest:19980112.
Oren, R., Sperry, J.S., Katul, G.G., Pataki, D.E., Ewers, B.E., Phillips, N., Schäfer, K.V.R., 1999. Survey and synthesis of intra- and interspecific variation in stomatal sensitivity to vapour pressure deficit. Plant Cell Environ. 22, 1515–1526. http://dx.doi.org/10.1046/j.1365-3040.1999.00513.x.
Oren, R., Zimmermann, R., Terbough, J., 1996. Transpiration in upper Amazonia floodplain and upland forests in response to drought-breaking rains. Ecology 77, 968–973. http://dx.doi.org/10.2307/2265517.
Patrimoine et répartition - Office National de l'Huile de Tunisie [WWW Document], 2017. URL http://www.onh.com.tn/index.php/fr/2016-05-23-14-44-46/l-olivier/patrimoine-et-repartition (Accessed 10 October 2017).
Phillips, R.E., Ronald, I., Phillips, E., 1984. plant available water and plant water stress. Plant Soil Sci. 5, 1–5.
Ramos, A.F., Santos, F.L., 2009. Water use, transpiration, and crop coefficients for olives (cv. Cordovil), grown in orchards in Southern Portugal. Biosyst. Eng. 102, 321–333. http://dx.doi.org/10.1016/j.biosystemseng.2008.12.006.
Reynolds, J.F., Kemp, P.R., Tenhunen, J.D., 2000. Effects of long-term rainfall variability on evapotranspiration and soil water distribution in the Chihuahuan desert: a modeling analysis. Plant Ecol. 150, 145–159. http://dx.doi.org/10.1023/A:1026530522612.
Romero, M.P., Jesús Tovar, M., Girona, Joan, Motilva, M.José, 2002. Changes in the HPLC phenolic profile of virgin olive oil from Young trees (Olea europaea L. Cv. Arbequina) grown under different deficit irrigation strategies. J. Agric. Food chem. 50. http://dx.doi.org/10.1021/JF020357H.
Roupsard, O., Bonnefond, J.M., Irvine, M., Berbigier, P., Nouvellon, Y., Dauzat, J., Taga, S., Hamel, O., Jourdan, C., Saint-André, L., Mialet-Serra, I., Labouisse, J.P., Epron, D., Joffre, R., Braconnier, S., Rouzière, A., Navarro, M., Bouillet, J.P., 2006. Partitioning energy and evapo-transpiration above and below a tropical palm canopy. Agric. For. Meteorol. 139, 252–268. http://dx.doi.org/10.1016/j.agrformet.2006.07.006.
Rousseaux, M.C., Figuerola, L.P., Correa-Tedesco, G., Searles, P.S., 2009. Seasonal variations in sap flow and soil evaporation in an olive (Olea europaea L.) grove under two irrigation regimes in an arid region of Argentina. Agric. Water Manag. 96, 1037–1044. http://dx.doi.org/10.1016/J.AGWAT.2009.02.003.
Salvucci, G.D., 1997. Soil and moisture independent estimation of stage-two evaporation from potential evaporation and albedo or surface temperature. Water Resour. Res. 33, 111–122. http://dx.doi.org/10.1029/96WR02858.
Sanchez, J.M., Kustas, W.P., Caselles, V., Anderson, M.C., 2008. Modelling surface energy fluxes over maize using a two-source patch model and radiometric soil and canopy temperature observations. Remote Sens. Environ. 112, 1130–1143. http://dx.doi.org/10.1016/J.RSE.2007.07.018.
Santos, F.L., Valverde, P.C., Reis, J.L., Ramos, A.F., Castanheira, N.L., 2012. Sap flow scaling and crop coefficient of dry-farmed olive orchards converted to irrigation. Acta Hortic. 231. http://dx.doi.org/10.17660/ActaHortic.2012.949.33.
Scanlon, T., Kustas, W.P., 2010. Partitioning carbon dioxide and water vapor fluxes using correlation analysis. Agric. For. Meteorol. 150, 89–99. http://dx.doi.org/10.1016/J.AGRFORMET.2009.09.005.
Schuurman, J.J., Goedewaagen, M.A.J., 1971. Methods for the Examination of Root Systems and Roots, 2nd ed. Pudoc, Wageningen.
Scott, R.L., Huxman, T.E., Cable, W.L., Emmerich, W.E., 2006. Partitioning of evapotranspiration and its relation to carbon dioxide exchange in a Chihuahuan Desert shrubland. Hydrol. Process. 20, 3227–3243. http://dx.doi.org/10.1002/hyp.6329.
Sepulcre-Cantó, G., Zarco-Tejada, P.J., Jiménez-Muñoz, J.C., Sobrino, J.A., Miguel, E., de, Villalobos, F.J., 2006. Detection of water stress in an olive orchard with thermal remote sensing imagery. Agric. For. Meteorol. 136, 31–44. http://dx.doi.org/10.1016/j.agrformet.2006.01.008.
Smith, D.M., Allen, S.J., 1996. Measurement of sap flow in plant stems. J. Exp. Bot. 47, 1833–1844. http://dx.doi.org/10.1093/jxb/47.12.1833.
Smith, S.D., Herr, C.A., Leary, K.L., Piorkowski, J.M., 1995. Soil-plant water relations in a Mojave Desert mixed shrubcommunity: a comparison of three geomorphic surfaces. J. Arid Environ. 29, 339–351. http://dx.doi.org/10.1016/S0140-1963(05)80113-2.
Song, L., Kustas, W.P., Liu, S., Colaizzi, P.D., Nieto, H., Xu, Z., Ma, Y., Li, M., Xu, T., Agam, N., Tolk, J.A., Evett, S.R., 2016. Applications of a thermal-based two-source energy balance model using Priestley-Taylor approach for surface temperature partitioning under advective conditions. J. Hydrol. 540, 574–587. http://dx.doi.org/10.1016/j.jhydrol.2016.06.034.
Sulman, B.N., Roman, D.T., Scanlon, T.M., Wang, L., Novick, K.A., 2016. Comparing methods for partitioning a decade of carbon dioxide and water vapor fluxes in a temperate forest. Agric. For. Meteorol 226–227, 229–245. http://dx.doi.org/10.1016/j.agrformet.2016.06.002.
Tataranni, G., Santarcangelo, M., Sofo, A., Xiloyannis, C., Tyerman, S.D., Dichio, B., 2015. Correlations between morpho-anatomical changes and radial hydraulic conductivity in roots of olive trees under water deficit and rewatering. Tree Physiol. 35, 1356–1365. http://dx.doi.org/10.1093/treephys/tpv074.
Teixeira, D.C.A.H., Bastiaanssen, W.G.M., 2012. Five methods to interpret field measurements of energy fluxes over a micro-sprinkler-irrigated mango orchard. Irrig. Sci. 30, 13–28. http://dx.doi.org/10.1007/s00271-010-0256-y.
Testi, L., Villalobos, F., Orgaz, F., 2004. Evapotranspiration of a young irrigated olive orchard in southern Spain. Agric. For. Meteorol. 121, 1–18. http://dx.doi.org/10.1016/j.agrformet.2003.08.005.
Tognetti, R., d'Andria, R., Lavini, A., Morelli, G., 2006. The effect of deficit irrigation on crop yield and vegetative development of Olea europaea L. (cvs. Frantoio Leccino). Eur. J. Agron. 25, 356–364. http://dx.doi.org/10.1016/j.eja.2006.07.003.
Tognetti, R., d'Andria, R., Morelli, G., Calandrelli, D., Fragnito, F., 2004. Irrigation effects on daily and seasonal variations of trunk sap flow and leaf water relations in olive trees. Plant Soil 263, 249–264. http://dx.doi.org/10.1023/B:PLSO.0000047738.96931.91.
Tognetti, R., Raschi, A., Beres, C., Fenyvesi, A., Ridder, H.-W., 1996. Comparison of sap flow, cavitation and water status of Quercus petraea and Quercus cerris trees with special reference to computer tomography. Plant Cell Environ. 19, 928–938. http://dx.doi.org/10.1111/j.1365-3040.1996.tb00457.x.
Vertessy, R.A., Benyon, R.G., O'Sullivan, S.K., Gribben, P.R., 1995. Relationships between stem diameter, sapwood area, leaf area and transpiration in a young mountain ash forest. Tree Physiol. 15, 559–567. http://dx.doi.org/10.1093/treephys/15.9.559.
Villalobos, F., Orgaz, F., Testi, L., Fereres, E., 2000. Measurement and modeling of evapotranspiration of olive (Olea europaea L.) orchards. Eur. J. Agron. 13, 155–163. http://dx.doi.org/10.1016/S1161-0301(00)00071-X.
Viola, F., Caracciolo, D., Pumo, D., Noto, L.V., 2013. Olive yield and future climate forcings. Procedia Environ. Sci. 19, 132–138. http://dx.doi.org/10.1016/j.proenv.2013.06.015.
Wagner, B., Tarnawski, V.R., Hennings, V., Müller, U., Wessolek, G., Plagge, R., 2001. Evaluation of pedo-transfer functions for unsaturated soil hydraulic conductivity using an independent data set. Geoderma 102, 275–297. http://dx.doi.org/10.1016/S0016-7061(01)00037-4.
Wahbi, S., Wakrim, R., Aganchich, B., Tahi, H., Serraj, R., 2005. Effects of partial root-zone drying (PRD) on adult olive tree (Olea europaea) in field conditions under arid climate. Agric. Ecosyst. Environ. 106, 289–301. http://dx.doi.org/10.1016/j.agee.2004.10.015.
Wang, L., Caylor, K.K., Villegas, J.C., Barron-Gafford, G.A., Breshears, D.D., Huxman, T.E., 2010. Partitioning evapotranspiration across gradients of woody plant cover: assessment of a stable isotope technique. Geophys. Res. Lett. 37http://dx.doi.org/10.1029/2010GL043228. n/a-n/a.
Williams, D.G., Cable, W., Hultine, K., Hoedjes, J.C.B., Yepez, E.A., Simonneaux, V., Er-Raki, S., Boulet, G., de Bruin, H.A.R., Chehbouni, A., Hartogensis, O.K., Timouk, F., 2004. Evapotranspiration components determined by stable isotope, sap flow and eddy covariance techniques. Agric. For. Meteorol. 125, 241–258. http://dx.doi.org/10.1016/j.agrformet.2004.04.008.
Wilson, K., Goldstein, A., Falge, E., Aubinet, M., Baldocchi, D., Berbigier, P., Bernhofer, C., Ceulemans, R., Dolman, H., Field, C., Grelle, A., Ibrom, A., Law, B., Kowalski, A., Meyers, T., Moncrieff, J., Monson, R., Oechel, W., Tenhunen, J., Valentini, R., Verma, S., 2002. Energy balance closure at FLUXNET sites. Agric. For. Meteorol. 113,

223–243. http://dx.doi.org/10.1016/S0168-1923(02)00109-0.
Wullschleger, S.D., Hanson, P., Todd, D., 2001. Transpiration from a multi-species deciduous forest as estimated by xylem sap flow techniques. For. Ecol. Manag. 143, 205–213. http://dx.doi.org/10.1016/S0378-1127(00)00518-1.
Xiao, Z., Lu, S., Heitman, J., Horton, R., Ren, T., 2012. Measuring subsurface soil-water evaporation with an improved heat-pulse probe. Soil Sci. Soc. Am. J. 76, 876. http://dx.doi.org/10.2136/sssaj2011.0052n.
Xu, Z., Zhou, G., Shimizu, H., 2010. Plant responses to drought and rewatering. Plant Signal. Behav. 5, 649–654. http://dx.doi.org/10.4161/PSB.5.6.11398.
Yamanaka, T., Yonetani, T., 1999. Dynamics of the evaporation zone in dry sandy soils. J. Hydrol. 217, 135–148. http://dx.doi.org/10.1016/S0022-1694(99)00021-9.
Zarco-Tejada, P.J., González-Dugo, V., Berni, J.A.J., 2012. Fluorescence, temperature and narrow-band indices acquired from a UAV platform for water stress detection using a micro-hyperspectral imager and a thermal camera. Remote Sens. Environ. 117, 322–337. http://dx.doi.org/10.1016/j.rse.2011.10.007.
Zeleke, K.T., Wade, L.J., 2012. Evapotranspiration estimation using soil water balance, weather and crop data. Evapotranspiration -Remote Sensing and Modeling. pp. 41–57.
Zhang, J.-G., Guan, J.-H., Shi, W.-Y., Yamanaka, N., Du, S., 2015. Interannual variation in stand transpiration estimated by sap flow measurement in a semi-arid black locust plantation, Loess plateau, China. Ecohydrology 8, 137–147. http://dx.doi.org/10.1002/eco.1495.
Zhao, W., Liu, B., 2010. The response of sap flow in shrubs to rainfall pulses in the desert region of China. Agric. For. Meteorol. 150, 1297–1306. http://dx.doi.org/10.1016/j.agrformet.2010.05.012.